

We are IntechOpen, the world's leading publisher of Open Access books Built by scientists, for scientists

6,900

Open access books available

186,000

International authors and editors

200M

Downloads

Our authors are among the

154

Countries delivered to

TOP 1%

most cited scientists

12.2%

Contributors from top 500 universities



WEB OF SCIENCE™

Selection of our books indexed in the Book Citation Index
in Web of Science™ Core Collection (BKCI)

Interested in publishing with us?
Contact book.department@intechopen.com

Numbers displayed above are based on latest data collected.
For more information visit www.intechopen.com



Pattern Synthesis in Time-Modulated Arrays Using Heuristic Approach

Sujit Kumar Mandal, Ananya Mukherjee, Sujoy Mandal and Tanmoy Das

Abstract

Time-modulation principle evolves as an emerging technology for easy realization of the desired array patterns with the help of an additional degree of freedom, namely, “time.” To the antenna community, the topic, time-modulated antenna array (TMAA) or 4D antenna arrays, has got much attention during the last two decades. However, population-based, stochastic, heuristic evolutionary algorithm plays as an important protagonist to meet the essential requirements on synthesizing the desired array patterns. This chapter is basically devoted to understand the theory of different time-modulation principles and the application of optimization techniques in solving different antenna array synthesis problems. As a first step, the theory of time-modulation principles and the behaviors of the sideband radiation (SBR) that appeared due to time modulation have been studied. Then, different important aspects associated with TMAA synthesis problems have been discussed. These include conflicting parameters, the need of evolutionary algorithms, multiple objectives and their optimization, cost function formation, and selection of weighting factors. After that, a novel approach to design a time modulator for synthesizing TMAAs is presented. Finally, discussing the working principle of an efficient heuristic approach, namely, artificial bee colony (ABC) algorithm, the effectiveness of the time modulator and potentiality of the algorithm are presented through representative numerical examples.

Keywords: antenna array synthesis, side lobe level (SLL), time modulation, sideband radiation, sideband level (SBL), evolutionary algorithms

1. Introduction

In any wireless communication system, the antenna is an essential component to transmit or receive a message signal. In many applications such as satellite communication, point-to-point communication, military communication, surveillance, radar, sonar, aircraft, etc., the antenna gain and directivity should be sufficiently high so as to direct most of the antenna-radiated power along a particular direction by reducing the power level (side lobe power) at other directions. A single radiator may not meet such requirements due to its omnidirectional power pattern and high side lobe level (SLL) in the far-field region. Moreover, radiation of huge amount of

transmitter power from a single antenna element needs high-power amplification in the feed network. The high-power amplifier is not easy to design and safe to handle. Therefore, a number of antenna elements are arranged along a line, called linear antenna array (LAA), or in a plane called planer antenna array (PAA). The use of multiple antenna elements in the transmission and reception systems simplifies the power amplifier design problem by reducing the power level per transmitting antenna elements of the arrays. Some other advantages of using antenna arrays are to improve signal fading resistance or deliberately exploit the signal fading; mitigate the interfering signal coming from other directions, adaptive beam forming, and null steering at both transmitter and receiver; and increase system capacity. Due to its high gain and narrow beamwidth, the large antenna arrays also find applications in weather forecast, astronomy, image processing, and biomedical imaging.

Although the antenna array with uniform excitation amplitude and equally spaced antenna elements is the simplest one for practical implementation and also can be used to synthesize different patterns, due to the high value of peak SLL, it is impractical to use in such applications. In conventional antenna array (CAA) system, the low side lobe pattern is obtained by tapering the static excitation amplitudes. The well-known analytical techniques to taper amplitude distributions in nonuniformly excited antenna arrays are Dolph-Chebyshev (DC) and Taylor series [1]. However, the high dynamic range ratio (DRR) and complex excitation of the antenna elements are the major drawbacks of such CAA synthesis method with nonuniform excitation, because the complex excitation is practically difficult to realize and designing the practical antenna with high DRR of static amplitude tapering provides various errors such as systematic errors and random errors.

Conversely, the ultralow SLL pattern in the far-field of the antenna array can be realized even in uniform amplitude antenna arrays by exploiting “time” as a fourth dimension [2, 3]. The introduction of the additional dimension “time,” into the antenna array system, results in time-modulated antenna array (TMAA). By using the fourth degree of freedom, “time” in antenna array system, various errors in realizing the low SLL pattern can be drastically reduced, and error tolerance levels become equivalent to those obtained in conventional antenna array system for the patterns of ordinary SLLs [4, 5]. Yet, the main disadvantage in TMAA is the generation of sideband signals which appeared due to the time modulation of the antenna signals by periodically commutating the antenna elements with the specified modulation frequency. Therefore, time modulation involves with the radiation or reception of electromagnetic energy at different harmonics of the modulation frequency that are termed as sidebands. In some applications where the antenna array is synthesized at center (operating) frequency, sideband signals are not useful. In such cases, sideband signals and associated power losses are suppressed to improve the radiation efficiency at the operating frequency of the antenna array [5, 6]. Presently, it is investigated that sideband signals are also effective in synthesizing multiple patterns and researchers are interested to exploit the same in some specific applications of the modern-day communication systems like harmonic beam forming [7], generation of multibeam radiation pattern [8], beam steering [9, 10], direction finding [11], wireless power transmission [12], etc. The interested readers may refer to Reference [13] for the state-of-the-art overview, applications, and present research trend on time-modulation theory and techniques.

This chapter explains about the fundamental theory and techniques of different time-modulation strategies and such antenna array synthesis methods using optimization algorithms. The parameters involved with the use of optimization techniques and TMAA synthesis problem have also been presented.

2. Theory of time-modulated antenna array (TMAA)

Let us consider a linear antenna array of N number of mutually uncoupled isotropic radiators with inter-element spacing d_0 . The antenna elements are placed along the x -axis with the first element at the origin of the geometrical coordinate system as shown in **Figure 1**. In the XZ plane (one of the vertical principle plane), the array factor expression of CAAs can be obtained as in Eq. (1) [1]:

$$AF^c = \sum_{p=1}^N A_p e^{j\Phi_p} e^{j[\omega_0 t + (p-1)\beta d_0 \cos \theta]} \quad (1)$$

where $\omega_0 = 2\pi f_0 = 2\pi/T_0$ is the angular frequency in rad/sec for the operating signal of frequency f_0 in Hz; T_0 is the time period of the operating signal; $\beta = 2\pi/\lambda$ is the wave number with λ being the wavelength; $p = 1, \dots, N$ represents the element number of the antenna array; A_p and $\Phi_p \forall p \in [1, N]$ stand for the normalized static excitation amplitudes and phases of the array elements, respectively; and θ is the angle made by the line joining the observing point and the origin with the x -axis as shown in **Figure 1**.

In order to control the antenna pattern by using the additional degree of freedom, namely, “time,” periodically the static excitation amplitudes of the antenna element are time-modulated. The commonly used and simplest way of doing that is to insert high-speed radio-frequency (RF) switches in the feed network, just prior to radiating sources as shown in **Figure 2**. Each array element is assumed to be connected to the RF switches with individually controlled switching circuits. The switches are periodically “on” and “off” according to a predetermined on-time sequence t_p^{on} ($0 \leq t_p^{on} \leq T_m$) $\forall p \in [1, N]$, with time period, T_m . The switching rate, $f_m = 1/T_m$, is selected such that if the maximum frequency of the message signal is f_{max} (Hz), $T_0 \ll T_m \leq \frac{1}{f_{max}}$ [14]. Thus, during each period, the on-time duration by which a switch is on, the array element connected to that switch is active for that time duration only; otherwise, it will be inactive.

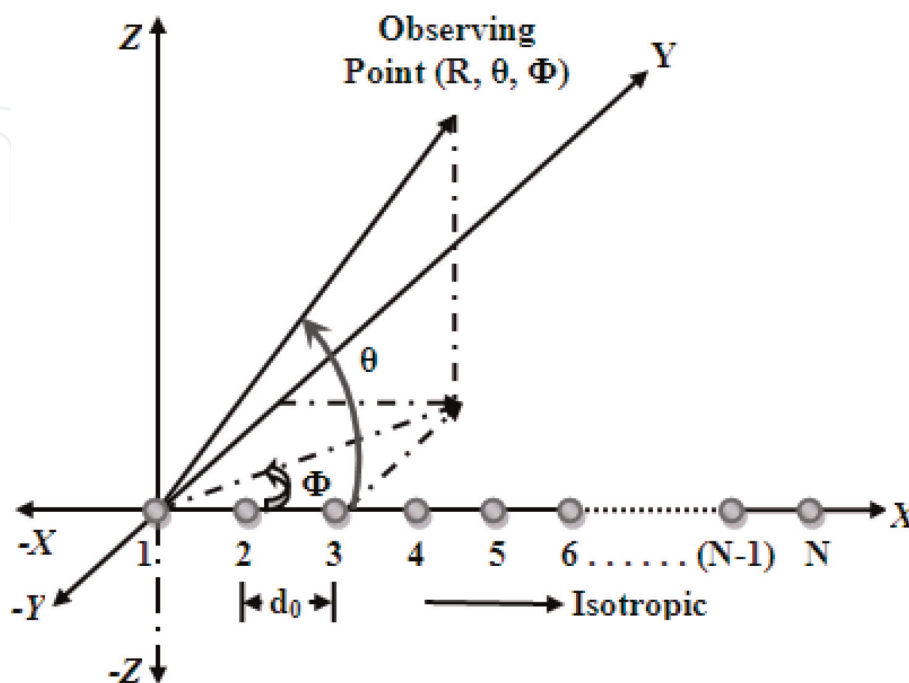


Figure 1.
 Basic antenna array of N element with inter-element spacing of d_0 .

Let us further assume that all the switches corresponding to the antenna elements in **Figure 2** are on (short circuited) at the same instant of time, say at the beginning of each period " $\eta * T_m$ " with " η " being the time period number 0, 1, 2, ... , by using rectangular pulses of amplitude unity. Hence, the switches which are on for the whole time period T_m as shown in **Figure 3(a)** can be directly connected to the signal as time modulation is not required for such cases. On the other hand, the switches remained short circuited for their specific on-time duration and open

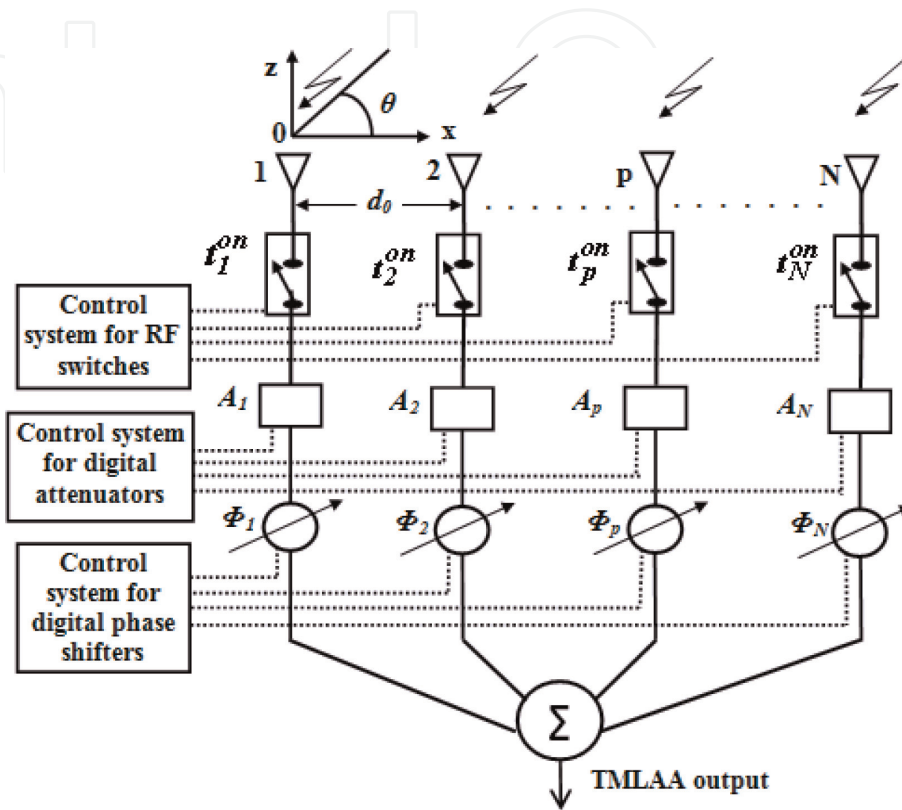


Figure 2.
Time-modulated linear antenna array (TMLAA) geometry.

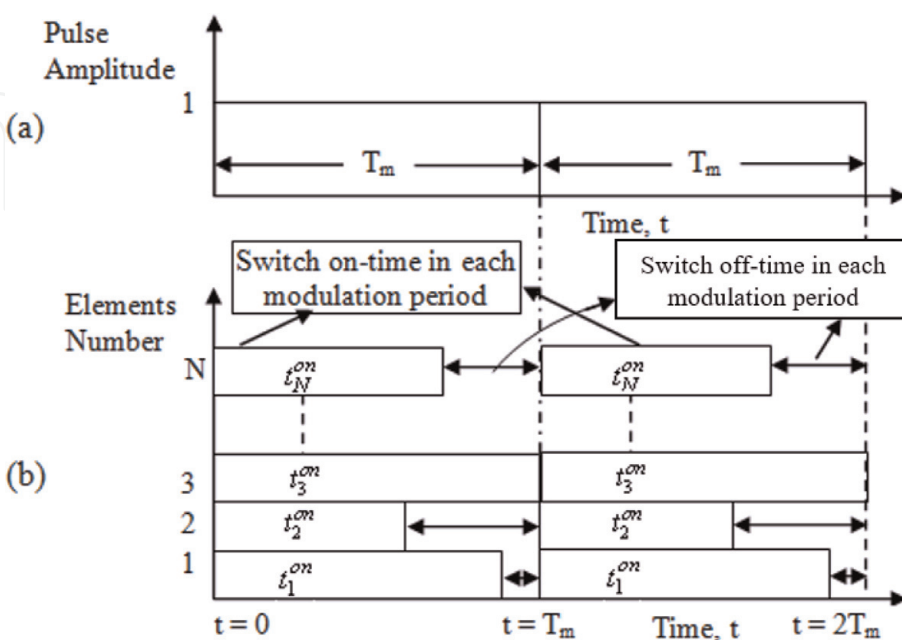


Figure 3.
The periodic pulse sequence of the TMLAA. (a) Unit pulse of periodicity T_P . (b) On-off time duration of each antenna elements for one time-modulation period T_P , and it is repeated at every T_P time interval.

circuited after their corresponding on-time duration (t_p^{on}) as shown in **Figure 3(b)**. **Figure 3(b)** shows the on–off time sequence of the switches for the first two time periods only. The same process is repeated in the next consecutive periods. Thus the switching function of the p^{th} element can be expressed by a periodic pulse $U_p(t)$, such that at each period

$$U_p(t) = \begin{cases} 1; & \eta T_m \leq t \leq (\eta T_m + t_p^{on}) \\ 0; & \text{elsewhere} \end{cases} \quad (2)$$

After the switching operation, the array factor expression of Eq. (1) can be written as in Eq. (3) [2]:

$$AF(\theta, t) = \sum_{p=1}^N U_p(t) A_p e^{j[\omega_0 t + \alpha_p + \Phi_p]} \quad (3)$$

where $\alpha_p = (p - 1)\beta d_0 \{ \cos \theta - \cos \theta_0 \}$ is the linear progressive phase shift of p^{th} element and θ_0 is the direction of maximum radiation. As $U_p(t)$ in Eq. (3) is a time periodic function of periodicity T_m , it can be decomposed by applying Fourier series technique as

$$U_p(t) = \sum_{k=-\infty}^{k=+\infty} C_{pk} e^{jk\omega_m t} \quad (4)$$

where $\omega_m = 2\pi/T_m = 2\pi f_m$ is the modulation frequency and C_{pk} is the Fourier coefficient at the k^{th} harmonics for the p^{th} element and is obtained as [5, 14]

$$C_{pk} = \tau_p \frac{\sin(k\pi\tau_p)}{k\pi\tau_p} e^{-jk\pi\tau_p} \quad (5)$$

where $\tau_p = t_p^{on}/T_m \forall p \in [1, N]$ stand for the normalized on-time durations of the array elements.

Putting Eq. (4) in Eq. (3), the array factor expression of Eq. (3) is obtained as

$$AF(\theta, t) = \sum_{k=-\infty}^{k=+\infty} \sum_{p=1}^N A_p C_{pk} e^{j(\Phi_p + \alpha_p)} e^{j(\omega_0 + k\omega_m)t} \quad (6)$$

Thus, Eq. (6) expresses that the signal is not only radiated at the operating frequency, ω_0 for $k = 0$, but also the signals are radiated at different harmonics of the modulating frequency, $k\omega_m$, with ω_0 as the center frequency. The signal radiation at different harmonics is termed as sideband radiation (SBR). For such a TMLAA, the array factor expression at k th harmonic of the modulation frequency is readily obtained by combining Eqs. (5) and (6) as

$$AF_k(\theta, t) = e^{j(\omega_0 + k\omega_m)t} \sum_{p=1}^N A_p \tau_p \frac{\sin(k\pi\tau_p)}{k\pi\tau_p} e^{-j[k\pi\tau_p - (\Phi_p + \alpha_p)]} \quad (7)$$

Therefore, the array factor at the fundamental frequency, i.e., at operating frequency (for $k = 0$) and at the first two positive harmonics (for $k = 1$ and $k = 2$), is obtained as in Eqs. (8), (9), and (10), respectively:

$$AF_0(\theta, t) = e^{j\omega_0 t} \sum_{p=1}^N A_p \tau_p e^{j(\Phi_p + \alpha_p)} \quad (8)$$

$$AF_1(\theta, t) = \frac{e^{j(\omega_0 + \omega_m)t}}{\pi} \sum_{p=1}^N A_p \sin(\pi \tau_p) e^{-j[\pi \tau_p - (\Phi_p + \alpha_p)]} \quad (9)$$

$$AF_2(\theta, t) = \frac{e^{j(\omega_0 + 2\omega_m)t}}{2\pi} \sum_{p=1}^N A_p \sin(2\pi \tau_p) e^{-j[2\pi \tau_p - (\Phi_p + \alpha_p)]} \quad (10)$$

From Eq. (8), it can be observed that $\tau_p, \forall p \in [1, N]$ provides an additional flexibility in synthesizing antenna array patterns. For example, making values of $\tau_p, \forall p \in [1, N]$ equivalent to that of the required static excitation to synthesize Dolph-Chebyshev or Taylor series pattern, low SLL patterns can be realized even with uniformly excited array with unit static excitation $A_p = 1, \forall p \in [1, N]$. Also, Eqs. (9) and (10) indicate that the harmonics radiated from different time-modulated elements are added together at frequencies in multiples of the modulation frequency, f_m , to produce resultant sideband signals.

3. Behaviors of sideband radiation (SBR)

It can be observed from Eqs. (7)–(10) that, due to time modulation, the sideband signals inherently appeared around the center frequency spaced in multiples of the modulation frequency. In this section, the characteristics of harmonic signal radiated by an arbitrary time-modulated element are observed by varying the normalized switch-on time for its complete range from 0 to 1. Then by defining relative and normalized sideband power, the effects of reducing SLL on the first null beamwidth (FNBW) and maximum sideband power level are observed.

3.1 Characteristics of harmonic radiations (HRs)

From Eq. (7), we can see that the array factor at different sidebands is the superposition of the harmonic signal radiated from the individual antenna element. Hence, sideband power pattern and total sideband power can be obtained from the harmonic characteristics of the time-modulated elements as expressed in Eq. (5). The normalized harmonic radiation of the individual time-modulated antenna element is given as [15]

$$h_{pk} = 20 \log_{10} |C_{pk}| / |C_{p0}| = \frac{\sin(k\pi\tau_p)}{k\pi\tau_p} \quad (11)$$

where h_{pk} is the normalized/relative harmonic radiation corresponding to the p^{th} element. The variation of normalized harmonic power of the first three harmonics ($k = 1, 2, \text{ and } 3$) with normalized switch-on time, τ_p , over its complete range (0, 1) is shown in **Figure 4**. As can be seen, at the lower value of τ_p , all $h_{pk\text{max}}$ are almost the same, and for $\tau_p \rightarrow 0$, all $h_{pk\text{max}}$ are exactly equal to 0 (zero) dB as it is expected from the Fourier series of unit impulse function. However, at the other extremes of τ_p , when $\tau_p \rightarrow 1$, all $h_{pk\text{max}} \rightarrow -\infty$, which is the predicted result as can be seen in Eqs. (5) to (10), with $k = 1, 2, \text{ and } 3$. Again there is no radiation at h_{p2} for $\tau_p = 0.5$ and at h_{p3} for $\tau_p = 0.3$ and 0.66 which can also be verified from Eq. (5) with $k = 1, 2, \text{ and } 3$. Thus, **Figure 4** indicates that the contribution of the harmonic component

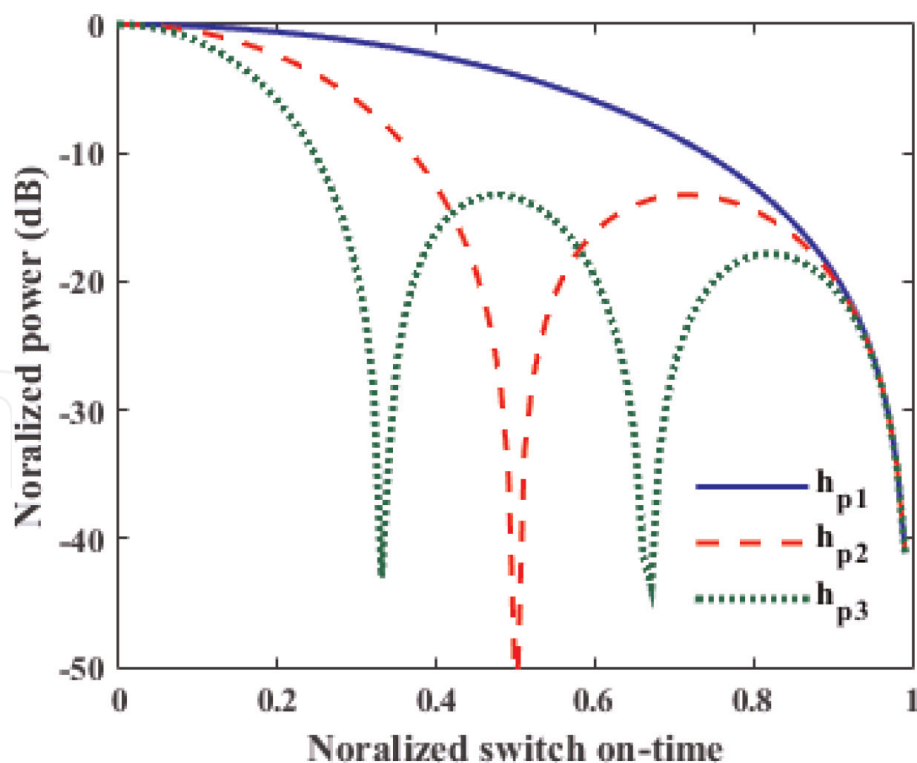


Figure 4.
 Variation of the first three harmonic powers from an antenna element with normalized switch-on time, τ_p .

from a particular element to produce the sideband pattern depends on the on-time duration of the corresponding element. Therefore, the desired sideband power pattern can be synthesized in TMAAs by judiciously controlling the on-time sequence of the time-modulated antenna elements.

3.2 Normalized and relative power

Usually in TMAA, the radiation pattern is synthesized at center frequency by suppressing the sideband radiation level to sufficiently low value. Thus, the maximum of the power radiated at f_0 is used to normalize the corresponding power pattern at center frequency. On the other hand, the sideband power is divided by the maximum power at f_0 to measure the relative power level at different sidebands with respect to that of the radiation at center frequency. In this regard, the relative signal power radiated at different harmonics ($k \neq 0$) is measured as in Eq. (12):

$$SBL_k(\text{dB}) = 20 * \log_{10}(AF_k(\theta, t) / \max(AF_0(\theta, t))) \quad (12)$$

where “ SBL_k ” represents the relative value of sideband level at k^{th} harmonic ($k = 1, 2, \dots$), i.e., relative value of the array factor AF_k in dB, and “ $\max(AF_0(\theta, t))$ ” is the maximum value of the array factor at operating frequency ω_0 , i.e., the maximum radiation level at $k = 0$. Thus, with $k = 0$, Eq. (11) gives the normalized power pattern for the center frequency pattern, whereas, for the sideband radiations (with $k \neq 0$), it is the relative power with respect to the maximum of the center frequency pattern.

3.3 Influence on the sideband level and first null beamwidth during reduction of side lobe level of the fundamental pattern

It is understood that in addition to the desired operating frequency (center frequency), TMAAs also radiate signals at the infinite number of different

harmonics of the modulation frequency. When the desired power pattern is synthesized at the center frequency, the sideband power is wasted. In this section, the influences on the first null beamwidth (FNBW) and sideband radiation by reducing SLL of the center frequency pattern are observed. The *SLL* of the power pattern at f_0 is reduced by using the conventional amplitude tapering technique, namely, Dolph-Chebyshev (DC) [1], and a heuristic search global optimization method, namely, genetic algorithm (GA) [16].

3.3.1 SLL reduction using Dolph-Chebyshev technique

The conventional antenna array synthesis technique such as Dolph-Chebyshev (DC) method [1] can be directly used to realize power pattern of the desired value of SLL at the center frequency. For a 30-element uniformly excited (UE) TMAA, the equivalent excitation coefficient of the DC pattern of desired SLL is made equal to the normalized on-time duration of the array elements. Following the DC method, the power pattern of different values of SLL is obtained at the center frequency.

3.3.2 SLL reduction using heuristic approach

In order to reduce the SLL at the center frequency pattern using optimization technique, a cost function is required. A well-defined cost function of any optimization problem is important to obtain satisfactory performance. The cost function measures the distances between the desired and obtained values of the radiation parameters which are to be controlled. During the optimization process, the algorithms compare the obtained values of the radiation parameters with those of their respective desired values. Without considering sideband radiation and FNBW, the cost function to realize the patterns of desired SLLs at f_0 is defined as

$$\Psi = (SLL_d - SLL_{max})^2 \quad (13)$$

where SLL_{max} is the actual value of the SLL as obtained during each trial of the optimization process and SLL_d is its desired value. Any heuristic search global optimization method can be employed to reduce the SLL of the power pattern at f_0 . Here, one of the useful stochastic search global optimization methods, namely, genetic algorithm (GA), is used to synthesize the power pattern of different values of SLL of the array under consideration [17].

3.3.3 Results and discussion

It can be seen from Eqs. (5)–(10) that the Fourier coefficients and hence amplitudes of the harmonic signals are decreasing gradually with increasing harmonic order. Thus, the radiation energy at the first few harmonics (called sidebands) is most significant. So, the influence on the maximum radiation at the first two harmonics of TMAA is observed by reducing the SLL of the center frequency pattern. Firstly, the SLL of the power pattern at f_0 is reduced by using the Dolph-Chebyshev (DC) method [1]. Then a global optimization method is used to synthesize the same pattern as obtained via DC. In order to observe the effects of reducing SLL on SBL and FNBW, these values are noted for different power patterns. **Table 1** shows the simulation results of the maximum sideband level (SBL_{max}) at the first and second harmonics for the fundamental pattern with different values of maximum SLL (SLL_{max}) ranging from -15 dB to -55 dB. The radiation pattern at f_0 as obtained by GA and DC with SLL of -55 dB is shown in **Figure 5**. The first null

The patterns at f_0 by DC				The patterns at f_0 by GA			
SLL_{max} (dB)	FNBW (deg)	$SBL_{1(max)}$ (dB)	$SBL_{2(max)}$ (dB)	SLL_{max} (dB)	FNBW (deg)	$SBL_{1(max)}$ (dB)	$SBL_{2(max)}$ (dB)
-15	7.2	-3.35	-8.30	-15.06	8.4	-10.01	-17.91
-20	8.4	-7.2	-17.83	-20.03	9.6	-9.95	-17.06
-25	9.8	-13.36	-20.25	-25.78	10.4	-8.51	-14.27
-30	11.2	-12.28	-19.31	-30.28	12.0	-9.98	-14.75
-35	12.4	-12.42	-17.45	-35.66	17.2	-12.19	-17.39
-40	13.8	-12.42	-17.45	-40.04	19.0	-6.058	-13.13
-45	15.2	-12.59	-17.40	-43.76	20.2	-10.12	-14.572
-50	16.6	-12.58	-17.40	-50.52	22.4	-7.301	-12.7870
-55	18.0	-12.55	-17.37	55.6	23.6	-7.3	-12.9

Table 1. Radiations maximum at the first two sidebands and FNBW for the fundamental patterns of different values of SLL.

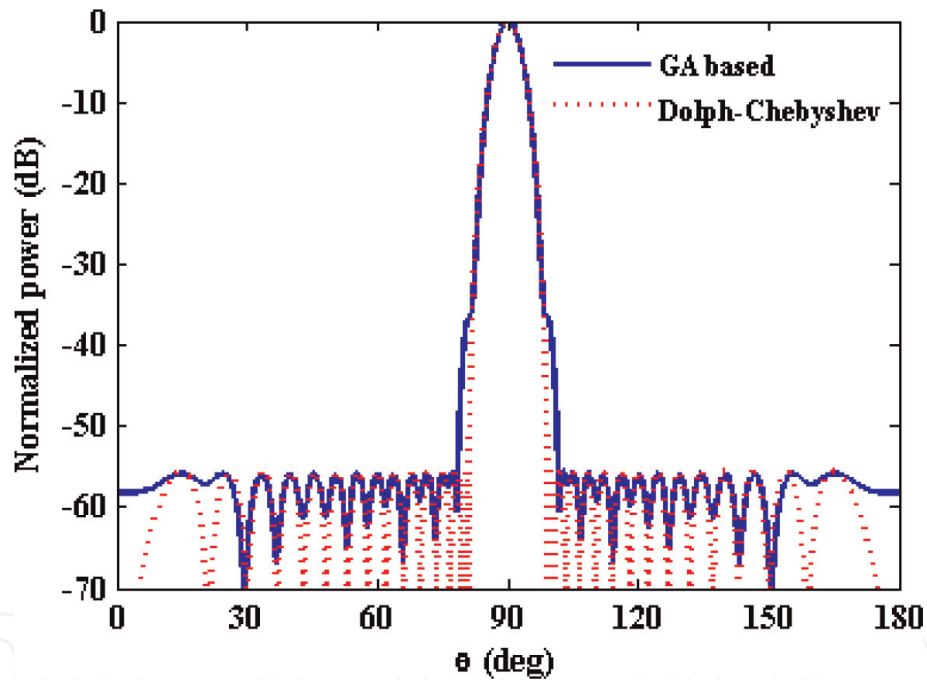


Figure 5. GA- and Dolph-Chebyshev-based pattern of SLL of -55.6 dB at f_0 .

beamwidth (FNBW) for different values of SLL_{max} of the main beam radiation pattern has been noted and is plotted in **Figure 6**. The maximum two harmonics are normalized with respect to the maximum value of the radiation at f_0 . For the different values of SLLs, the change in SBL_{max} at the first and second harmonics is shown **Figure 7**. Since, the Dolph-Chebyshev (DC) method gives the optimum pattern, i.e., the pattern with minimum FNBW for a specific value of SLL or vice versa. For the DC patterns of different SLLs, the corresponding FNBW, $SBL_{1(max)}$, and $SBL_{2(max)}$ are also given in **Table 1**. The plot SLL vs. FNBW is shown in **Figure 6**, and that for SLL vs. SBL_{max} is shown in **Figure 7**. **Figure 6** depicts that for the DC method, FNBW is linearly increased when $|SLL_{max}|$ is enhanced, whereas **Figure 7** shows that SBL_{1max} initially decreases from -3.35 dB and obtained its minimum value of -13.36 dB at -25 dB SLL pattern. Thereafter, it gradually

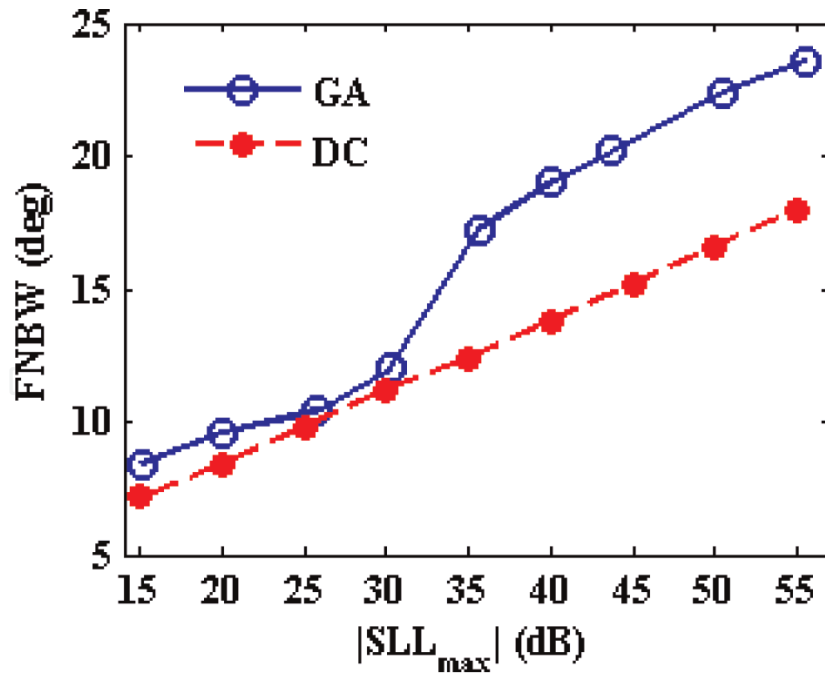


Figure 6. FNBW for different values of SLLs of the GA and Dolph-Chebyshev patterns at f_o .

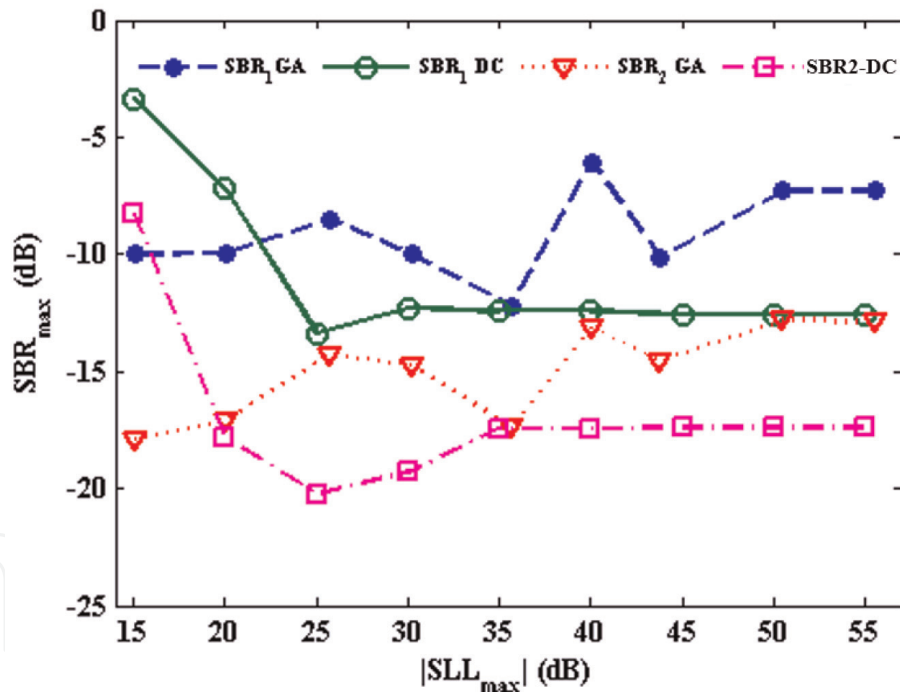
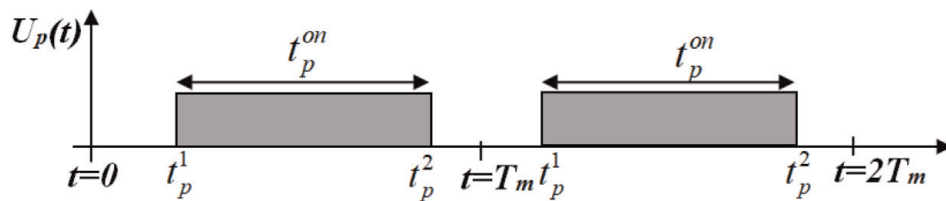


Figure 7. The plot of $SBR_{1(max)}$ and $SBR_{2(max)}$ for the different values of SLLs of the patterns at f_o .

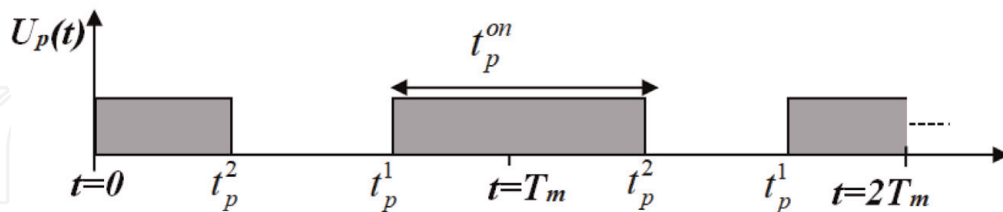
increases and becomes almost steady at -12.5 dB after -30 dB SLL. From **Figures 6** and **7**, it can be seen that for the GA-based patterns of different SLLs, SBL_{max} and $FNBW$ vary randomly as in the cost function, only SLL is considered without controlling $FNBW$ and SBL.

4. Time-modulation strategies

Different time-modulation strategies have been reported for synthesizing antenna arrays. These can be classified as (1) variable aperture size (VAS); (2) pulse



(a)



(b)

Figure 8.
 Switching instants defining pulse shifting strategy under two cases.

shifting; (3) binary optimized time sequence (BOTS); (4) subsectional optimized time steps (SOTS); (5) variable aperture size (VAS) with quantized on-time (VAS-QOT) or quantized aperture size (QAS); and (6) nonuniform period modulation (NPM). From the array factor expression as given in Eq. (6), it can be observed that for TMAA, the array factor at different harmonic can be obtained if the Fourier coefficients of different time-modulated elements are known. Therefore, in the following sections, along with the brief description of different time-modulation approaches, the Fourier coefficients of time switching elements under the respective time-modulation scheme are presented.

4.1 Variable aperture size (VAS)

This is the first type of time-modulation strategy as reported in [2] where the aperture size of the antenna array is varied with time. The time-modulation principle as discussed in Section 2 falls under this category.

4.2 Time modulation through pulse shifting

In VAS time-modulation scheme, only the switch-“on” time duration is considered for deriving the array factor expression. However, when the RF switches are used to commutate the antenna elements in TMAAs, the radiation patterns at center frequency as well as at different harmonics depend not only on the switch-on time duration but also on the switch-“on” and switch-“off” time instants of the array elements [18, 19]. Thus along with the switch-on time durations as considered in VAS scheme, switch-on and switch-off time instants are also taken as another degree of freedom to control the power pattern in TMAA. For the pulse shifting strategy, periodic switching instants of the p^{th} element over the modulation period are shown in **Figure 8**. In this case, both on-time instant t_p^1 and off-time instant t_p^2 can be controlled independently such that individually t_p^1 and $t_p^{\text{on}} = t_p^2 - t_p^1$ should be $\leq T_m$. Thus, two situations may occur. The first case is shown in **Figure 8(a)** where $t_p^1 < t_p^2$ and $t_p^1 + t_p^{\text{on}} \leq T_m$. Therefore, the switching function as expressed in Eq. (2) for VAS will be modified and is represented as in Eq. (14):

$$U_p(t) = \begin{cases} 1; & (\eta T_m + t_p^1) \leq t \leq (\eta T_m + t_p^2) \leq (\eta + 1)T_m \\ 0; & \text{elsewhere} \end{cases} \quad (14)$$

Hence, the normalized switch-on time duration, τ_p , is given as $\tau_p = \frac{t_p^{on}}{T_m} = \frac{t_p^2 - t_p^1}{T_m}$. Thus, the pulse shifting strategy reduces to VAS with $t_p^1 = 0$.

Another possible situation may appear as shown in **Figure 8(b)** where $t_p^1 > t_p^2$ and $t_p^1 + t_p^{on} \geq T_m$. Under such situation, the switching operation can be expressed as in Eq. (15):

$$U_p(t) = \begin{cases} 1; & (\eta T_m + t_p^1) \leq t \leq (\eta + 1)T_m \text{ and } (\eta + 1)T_m \leq t \leq \{(\eta + 1)T_m + t_p^2\} \\ 0; & \text{elsewhere} \end{cases} \quad (15)$$

The complex Fourier coefficient for the pulse shifting strategy at k^{th} harmonic due to the p^{th} element under the two cases can be obtained, respectively, as [14].

$$\text{Pulse shifting (Case 1)} C_{pk} = t_p^{on} \frac{\sin(k\pi t_p^{on})}{k\pi t_p^{on}} e^{-jk\pi(t_p^{on} + 2t_p^1)} \quad (16)$$

$$\text{Pulse shifting (Case 2)} C_{pk} = \frac{1}{k\pi} \left\{ \begin{array}{l} \sin[k\pi(1 - t_p^1)] e^{-jk\pi(1 + t_p^1)} + \\ \sin[k\pi(t_p^1 + t_p^{on} - T_m)] e^{-jk\pi(t_p^1 + t_p^{on} - T_m)} \end{array} \right\} \quad (17)$$

By taking into account the additional degree of freedom, namely, on-time instants of the antenna elements, improved array patterns can be observed. For example, more sideband reduction as compared to VAS approach is obtained when the same array pattern is synthesized at the center frequency [18–19], and electronic beam steering [9] and harmonic beam patterns of different shapes [7, 8] can be realized without phase shifters.

4.3 Binary optimized time sequence (BOTS)

In binary optimized time sequence (BOTS), the switch-on time duration of an arbitrary p^{th} element is divided into Q number of minimal time steps of equal length over a modulation time period T_m [20] as shown in **Figure 9**. The minimal time step, t^0 , is given by

$$t^0 = t^1 = t^2 = \dots = t^q = \dots = t^Q \quad (18)$$

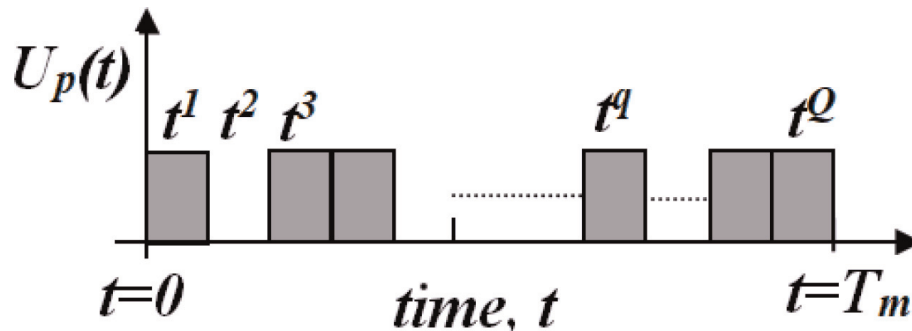


Figure 9
Switching function defining binary optimized time sequence (BOTS) strategy.

The periodic on–off sequence of the set of time steps corresponding to the p^{th} element is represented by the switching function $U_p(t)$. If the on–off status of q^{th} time step for the p^{th} element is symbolized with a binary bit, b_p^q , for which “on” status corresponds to $b_p^q=1$ and that for “off” status $b_p^q=0$, then the set of time steps for the p^{th} element is given as $b_p^1 b_p^2 b_p^3 \dots b_p^Q$. In order to synthesize the desired pattern, the optimal binary arrangement of the bit patterns, i.e., set of time steps to be under on states and off states, can be found by employing simple genetic algorithm (SGA) [16]. Considering each time step, b_p^q , as a gene, then on–off time sequence of N array elements represents the chromosome (χ) of GA and is given as

$$\chi = b_1^1 b_1^2 b_1^3 \dots b_1^Q b_2^1 b_2^2 b_2^3 \dots b_2^Q \dots b_p^1 b_p^2 b_p^3 \dots b_p^Q \dots b_N^1 b_N^2 b_N^3 \dots b_N^Q \quad (19)$$

The complex Fourier coefficient of p^{th} element at k^{th} harmonic with the BOTS switching scheme can be obtained as [20]

$$BOTS : C_{pk} = \frac{\sin(k\pi\tau_0)}{k\pi} \sum_{q=1}^Q b_p^q e^{-jk\pi\tau_0(2q-1)} \quad (20)$$

where $\tau_0 = \frac{t^0}{T_m}$ is the normalized time step. Thus, by incorporating more number of the degrees of freedom as the optimization variables to the evolutionary algorithm, the radiation pattern characteristics like SLL, SBL, SBR, etc. can be controlled skillfully.

4.4 Subsectional optimized time steps (SOTS)

In SOTS-based switching strategy, the time-modulation period (T_m) is divided into a number of subsections with variable lengths [21]. Let us assume that T_m is divided into Q number of time steps as shown in **Figure 10** for the switching strategy of p^{th} element of the array. For the q^{th} time step, the on and off time instants of the switch are denoted by $t_p^{q_{on}}$ and $t_p^{q_{off}}$, respectively, and the resultant on-time duration at q^{th} step is obtained as $t_p^q = t_p^{q_{off}} - t_p^{q_{on}}$. Therefore, the periodic time switching pulse $U_p(t)$ for the different time steps over a complete modulation period is represented as

$$U_p(t) = \begin{cases} 1; & 0 \leq t_p^{q_{on}} \leq t \leq t_p^{q_{off}} \leq T_m : \quad \forall q \in [1, Q] \\ 0; & \text{elsewhere} \end{cases} \quad (21)$$

The Fourier coefficient at the k^{th} harmonics for the p^{th} element can be written as

$$C_{pk} = \sum_{q=1}^Q \frac{(t_p^{q_{off}} - t_p^{q_{on}})}{T_m} \text{sinc}\left(k\omega_m(t_p^{q_{off}} - t_p^{q_{on}})\right) e^{-jk\omega_m(t_p^{q_{on}} + t_p^{q_{off}})} \quad (22)$$

where $\omega_m = \frac{2\pi}{T_m}$ denotes the modulation frequency used for the time modulation.

It can be observed that, if the number of subsections Q is 1, then SOTS is transformed into pulse shifting-based strategy. On the other scenario, if the on-time duration at each step, i.e., the separation between the on and off time instants, becomes multiples of $\frac{T_m}{Q}$, then SOTS takes the form of BOTS. So, SOTS-based switching strategy provides more flexibility in the design of optimized time sequences as compared to the other abovementioned switching strategies. However such improved flexibility in synthesizing the pattern is obtained at the cost of some

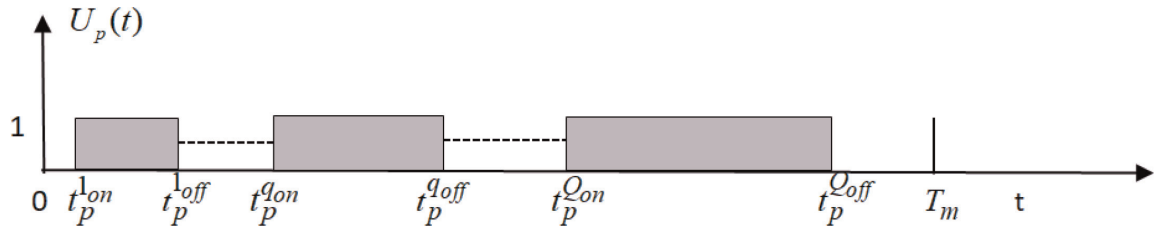


Figure 10. The schematic of the periodic pulse sequence for SOTS switching strategy of the p^{th} element of TMLAA.

increased design complexity, because realization of the number of unequal subsections with smaller section over the modulation period needs faster switching operation.

4.5 Quantized aperture size (QAS)

In Section 3, the different patterns of desired values of SLL at f_0 are obtained by making the on-time sequence equal to the Dolph-Chebyshev coefficient of the corresponding patterns. Thus the appropriate set of on-time sequence is required to generate the desired pattern even in uniformly excited TMAAs.

In this section, to generate different patterns in time-modulated antenna arrays (TMAAs) instead of considering continuous value of on-time duration [22], the modulation period is divided into a number of equal steps as in BOTS. However, in BOTS, multiple switching of on–off over the modulation period is considered. Such multiple changes of switching states over the modulation period need fast and complex switching circuit. Unlike BOTS, in this modulation scheme, the on–off states of the switches are assumed to change once over the complete modulation period like VAS. However, the on–off states of the switches are rounded off to the nearest quantization step to obtain quantized on-times (QOTs) of the corresponding elements as shown in **Figure 11**. In this time-modulation scheme, the time-modulation period, T_m , is quantized into “Q” number of discrete levels. At q^{th} quantization level, the value of t_q is given by $q^*(T_m/Q)$, where $q = 1, 2 \dots Q$. The allowable on-time t_p^{on} of the p^{th} array elements is taken as t_q with $q = 1, 2 \dots Q$ during each modulation period. Similar to the previously reported VAS time-modulation technique in which the continuous values of on-time durations are optimized to synthesize the desired pattern, this approach is defined as VAS with quantized on-time (VAS-QOT) or simply “quantized aperture size” (QAS) time modulation as the aperture size changes with quantized values of on-time durations of the elements.

4.6 Nonuniform period modulation (NPM)

In all of the abovementioned switching strategies, all antenna elements are modulated with the same modulation frequency, ω_m , and such time modulation is

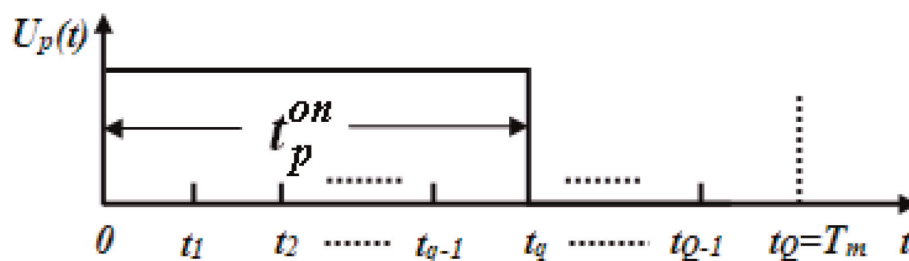


Figure 11. The proposed time-modulation approach for the quantized on-time of the switches.

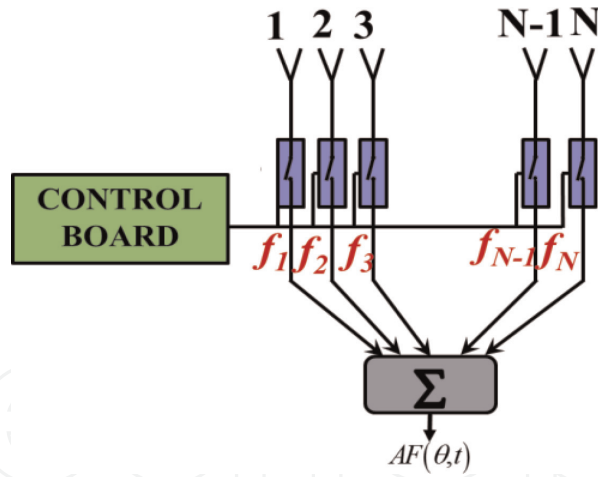


Figure 12.
 Time-modulated array architecture with NPM switching strategy where $f_1 \neq f_2 \neq \dots \neq f_N$.

termed as uniform period modulation (UPM). Time-modulated antenna array (TMAA) based on UPM is commonly known as uniform TMAA (UTMAA). On the other hand, if the antenna elements of the array are time-modulated with different modulation frequencies as shown in **Figure 12**, it is defined as time modulation with nonuniform period modulation (NPM), and the corresponding array is defined as nonuniform TMAA (NTMAA) [23–24]. Let us consider that the antenna elements are modulated with different modulation periods $T_p : \forall p \in [1, N]$ having modulation frequency $f_p = \frac{1}{T_p} : \forall p \in [1, N]$, where T_p and f_p , respectively, denote the modulation period and frequency of the p^{th} antenna element of the array. The periodic switching pulse of the p^{th} antenna element $U_p(t)$ is written as

$$U_p(t) = \begin{cases} 1; & t_p^1 < t \leq t_p^2 \\ 0; & 0 < t \leq t_p^1 \text{ or } t_p^2 < t \leq T_p \end{cases} \quad (23)$$

where t_p^1 and t_p^2 denote the on-time and off-time instant of the RF switch used to time modulate the p^{th} antenna element.

And finally, Fourier coefficient at the k^{th} harmonics for the p^{th} element is obtained as [24].

$$C_{pk} = \frac{\sin \left\{ k\pi f_p (t_p^2 - t_p^1) \right\}}{k\pi} e^{-jk\pi f_p (t_p^2 + t_p^1)} \quad (24)$$

Let $\tau_p = f_p (t_p^2 - t_p^1) = f_p t_p^{on}$ denote the normalized switch-on time duration, and then the corresponding array factor expression is written as

$$AF(\theta, t) = e^{j\omega_0 t} \sum_{p=1}^N A_p \tau_p e^{j(\Phi_p + \alpha_p)} + \sum_{\substack{k=-\infty, \\ k \neq 0}}^{\infty} \sum_{p=1}^N A_p \frac{\sin \left\{ k\pi f_p t_p^{on} \right\}}{k\pi} e^{-jk\pi f_p (2t_p^1 + t_p^{on})} e^{j2\pi(f_0 + kf_p)t} e^{j(\Phi_p + \alpha_p)} \quad (25)$$

where $\omega_0 = 2\pi f_0$ denotes the center frequency of the array.

The first summation indicates that the signals radiated at the center frequency ω_0 are accumulated in the space, whereas the second summation is due to the signals radiated at different harmonics. Now, if the modulation frequencies of the antenna elements are selected in such a way that $f_1 = f_2 = \dots = f_N = f_m$, then the scenario becomes UTMAA, and the term kf_p in the second summation becomes kf_m that means that the k^{th} -order harmonics of all the elements appeared at the same frequency. The scenario is the same for all other order of harmonics. As a result, radiated signals at the same frequency are accumulated in space, which in turn increases the resultant SBL.

But in the case of NTMAA, the modulation frequencies are selected in such a way that $f_1 \neq f_2 \neq \dots \neq f_N$. So, due to different modulation frequencies of different antenna elements, the signals radiated from different harmonics appeared at different frequencies, and the term kf_p in the second summation of [25] becomes different for different elements. That means the k^{th} -order harmonics of different elements appear at different frequencies and the scenario is the same for all the other order harmonics. So, unlike UTMAA, the harmonic signals appeared at different frequencies and are distributed in space, which in turn decreases the resultant SBL [23]. Recently, some research works have reported the calculation of the sideband power of NTMAA [24–25], and also the reduction of the sideband power losses using NTMAA is investigated [26].

5. Synthesis of time-modulated antenna arrays

5.1 Pattern synthesis parameters

In Section 3.3, it is observed that, though the conventional amplitude tapering methods such as Dolph-Chebyshev and Taylor series can be used to obtain the power pattern of the desired SLL with minimum beamwidth at the operating frequency of time-modulated antenna arrays, these methods are not useful to control the undesired power radiated at different sidebands. Similarly, it is also observed that application of the stochastic computational technique, such as GA, for suppressing side lobe level of the center frequency pattern without taking into account the sideband radiation, cannot reduce sideband signal power. Also, the beamwidth of such patterns is unpredictable. The power pattern with low SLL and suppressed sideband is preferred for the different communication systems.

Therefore, the parameters to be considered to synthesize pencil beam pattern in TMAAs as shown in **Figure 5** are SLL, FNBW, and SBL. However for the shaped beam pattern such as flattop and cosec squared, in addition to these three parameters, ripple level in the desired shaped region is another parameter to be taken into account. Further, it can be observed that while SLL is reduced, FNBW is increased and SBL is significantly large. In this regard, SLL, SBL, and FNBW for pencil beam pattern and SLL, SBL, FNBW, and ripple level for synthesizing shaped beam patterns are the conflicting parameters.

5.2 Multiple objectives

In Eq. (13), the cost function is defined to synthesize the power pattern with a single objective that is to achieve the desired value of SLL in the synthesized power pattern. Conversely, the synthesized pencil beam patterns at the operating frequency should have reduced SLL along with sufficiently suppressed SBL and narrow beamwidth. Thus, TMAA synthesis problems are multi-objective optimization problems where the multiple objectives are low SLL and narrow beamwidth (BW)

of the main beam at operating frequency and low value of maximum sideband level (SBL_{max}) for synthesizing pencil beam pattern while one more objective is low ripple level for synthesizing shaped beam patterns.

5.3 The need of evolutionary algorithm

TMAA synthesis problem is non-convex and nonlinear in nature. A number of numerical techniques as already mentioned—Dolph-Chebyshev and Taylor series [1]—are available to synthesize pencil beam power pattern in conventional antenna arrays (CAAs). Also, some analytical methods are reported to generate shaped beam patterns and phase-only controlled multiple power patterns in CAAs [27, 28, 29]. Durr et al. described a modified Woodward-Lawson technique to design phase-differentiated multiple pattern antenna arrays with prefixed amplitude distributions [27]. The analytical technique reported in [28] is used to determine the nonlinear phase distribution of linear arrays. A method based on projection approach [29] is proposed to synthesize reconfigurable array antennas of a cosecant² beam and a flattop beam (FTB) by using a common amplitude with phase-only control of analog phase shifters. Though these numerical and analytical techniques can also be applied to determine the nonlinear distributions of dynamic excitation coefficient and phase to synthesize power pattern at operating frequency of TMAAs, such methods have no control on sideband power level. Therefore, the powerful global stochastic optimization tools such as genetic algorithm (GA) [30], differential evolution (DE) [4–5, 31, 32], particle swarm optimization (PSO) [7], simulated annealing (SA) [6, 33], and artificial bee colony (ABC) [22, 34] are essentially required to solve such multi-objective TMAA synthesis problems.

5.4 Cost function with multiple objectives

Most of the TMAA synthesis problems are solved by applying single-objective optimization method where all the objectives are added with different weighting factors to form a single cost function and the cost function is minimized by employing heuristic evolutionary algorithms. The different stochastic optimization techniques are used with the objective to synthesize desired patterns at the operating frequency by reducing SLL and SBL . One of the commonly used techniques to define the cost function of such conflicting multi-objective TMAA synthesis problem is as expressed in Eq. (26):

$$\psi(\chi) = \sum_{h=0}^{h=V} W_h \cdot H(\delta_{hd} - \delta_h) \cdot (\delta_{hd} - \delta_h)^\rho \quad (26)$$

where χ is the set of unknown parameters, termed as optimization parameter vector which is to be determined by the used evolutionary algorithm; δ_h with $h = 0, 1, 2, \dots, V$ are the different parameters of the desired patterns; and δ_{hd} are the desired values of the specific parameters. For example, δ_0 is the maximum SLL (SLL_{max}) of the pattern at f_0 , δ_1 is the maximum of sideband radiations (SBR_{max}) among the first five sidebands, and δ_2 represents FNBW. “ W_h ” is the weighting factors for the corresponding terms. $H(\cdot)$ is the Heaviside step function. “ ρ ” is any natural number. It can be seen from Eqs. (13) and (26) that when the obtained values of δ_h are close to their desired values, the cost function value is moving toward zero. Thus, reaching zero value of the cost function confirms that the synthesized pattern satisfies the requirements in terms of the desired values of the intended synthesizing parameters. To illustrate the effectiveness of the cost

function as defined in Eq. (26), three multi-objective TMAA synthesis problems have been solved in Section 8. It is to be noted that, for different switching techniques, there is a trade-off between sideband level (*SBL*) and radiated total sideband power (*SRP*). Reducing the sideband level usually does not guarantee the power reduction. Hence, in that case a power term should be added into cost function.

5.5 Selection of weighting factors

In Eq. (26), all the objectives are added with different weighting factors to form a single cost function. In such techniques, it is tedious and difficult to select proper weighting factor for the optimal solution. Improper set of weighting factors strongly effect on achieving the final values of the desired synthesizing parameters and hence on the performance of the optimization algorithm. Generally, some selected best results are presented without mentioning such difficulties. However, these values of the weighting factors are obtained by trial and error method [4]. Though multi-objective evolutionary algorithm (MOEA) [35, 36] can be used to solve such problems, the researchers are not comfortable with it as it has been used rarely as compared to single-objective optimization approaches.

5.6 Evolutionary algorithms

It is already discussed that time-modulated antenna array synthesis problems are non-convex as well as nonlinear. Therefore, stochastic, global computational techniques are required to solve such problems. In this regard, different population-based global searching techniques such as DE, SA, GA, PSO, ABC, and multi-objective evolutionary algorithm (MOEA) have been applied successfully to synthesize the desired pattern at the center frequency by suppressing sideband radiation to satisfactorily low levels. However, here the working principle of ABC and its implementation have been presented, and a novel approach to synthesize TMAA is discussed.

6. A quantized time modulator (QTM) to synthesize different patterns in TMAAs

In Section 4.5, the quantized aperture size (QAS) time modulation or variable aperture size with quantize on-time duration has been explained. In this section first to realize such time-modulation approach, a time modulator, namely, quantized time modulator (QTM), is presented. Then it is shown that though the quantized on-time duration has been used, however, by selecting a suitable number of quantization levels, the effect of quantization errors on the synthesized patterns can be reduced. In order to select the best possible set of quantized on-time values, the potentiality of artificial bee colony algorithm (ABC) has been exploited as the global searching algorithm. Thus, for the desired patterns, ABC finds the optimum set of unknown parameter values from the discrete search space of QOT. The synthesized results as obtained by using this quantized on-time are compared with that achieved by using continuous search space of on-time [6, 33]. Finally, considering the discrete search space of QOT, a low side lobe level (SLL) flattop pattern with low dynamic range ratio (DRR) is synthesized by utilizing a fully digitally controlled QTM. The major advantage of this approach is that by implementing the “time modulator” either as a discrete component on a printed circuit board or in an integrated circuit (IC), it can generate different patterns in the TMAA system.

6.1 Quantized time modulator (QTM)

For appropriate switching operation at p^{th} element, a current pulse with a pulse width of t_p^{on} is required [2]. The proposed scheme for the periodical switching of the antenna array elements is shown in **Figure 13**. The QTM has two parts, namely, quantized pulse generator (QPG) and pulse width selector (PWS). In QPG, the consecutive tap delay output line, TAP_i with $i = 1, 2, \dots, Q$, introduces an equal delay of " T_m/Q ." The pulse output from the pulse generator (PG) is used to set the

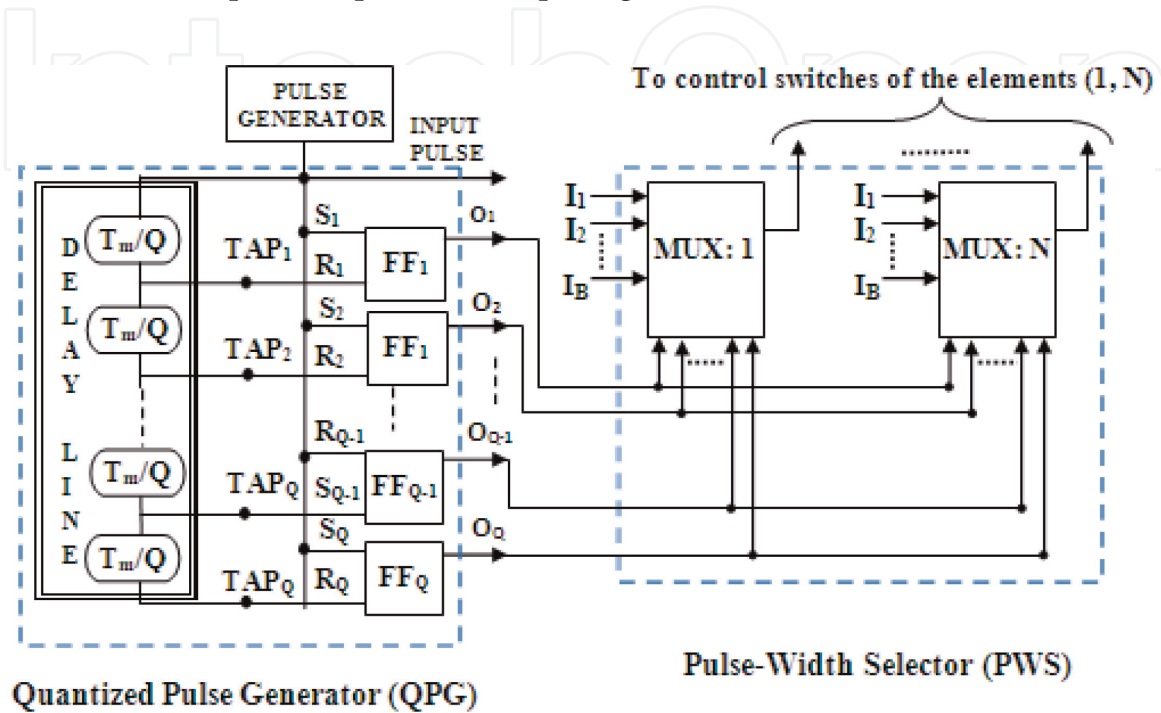


Figure 13.
 The proposed quantized time modulator (QTM).

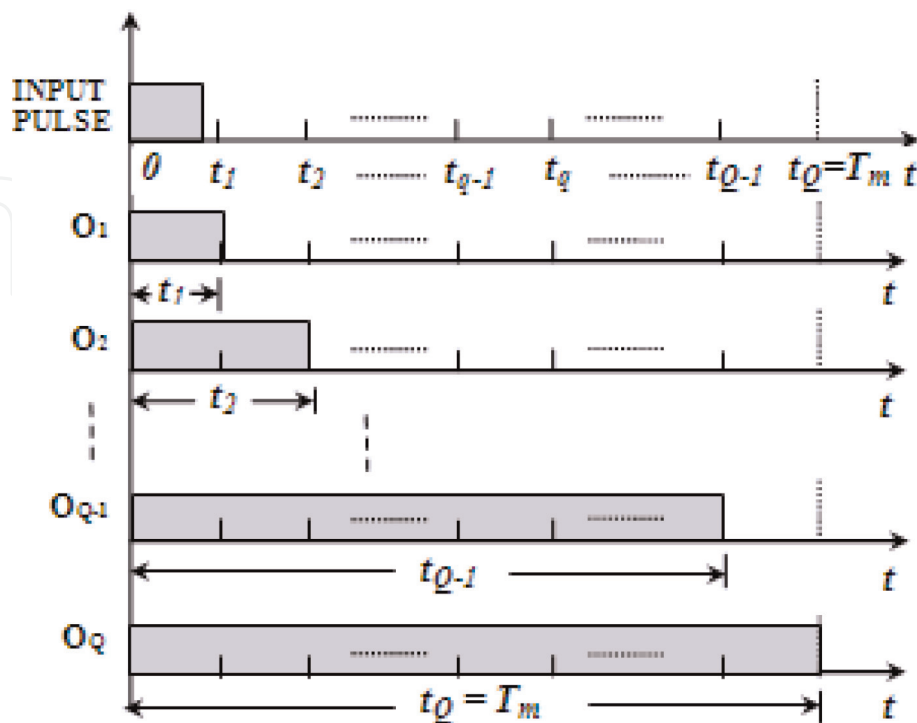


Figure 14.
 The wave form of the input and output pulses of different pulse widths that can be obtained at the outputs $O_q \forall q \in (1, \dots, Q)$ in **Figure 13**.

flip-flop (FFs) outputs to logic level **1**, whereas the delayed pulses from the corresponding tap outputs of the delay line are applied to reset the flip-flop outputs to logic level **0**. To avoid the simultaneous appearance of PG output and its delayed version at the S and R inputs of i^{th} flip-flop, respectively, the pulse width less than T_m/Q can be used. The current waveforms of the input pulse applied to the set (S) inputs of the flip-flops and output pulses appeared at the outputs O_q with $q = 1, 2, \dots, Q$ of different flip-flops as shown in **Figure 14**. Therefore, the QPG, consisting of a pulse generator, simple tapped delay line, and flip-flops, provides the required current pulses with quantized values of t_p^{on} .

One of the most important features in TMAAs is to reconfigure different antenna patterns just by changing the on-time sequence across each element. Such a feature can easily be obtained in the proposed QTM employing PWS. The PWS consists of N number of $(Q \times 1)$ multiplexers and their outputs that are used to modulate antenna element using the quantized values of t_p^{on} . With appropriate bit combination at the select inputs I_0, I_1, \dots, I_B of the multiplexers, one of the quantized pulses at the output of QPG is selected to time modulate the corresponding antenna element. Thus, just by using the appropriate combination of the select lines of multiplexers, it is very easy to reconfigure different patterns.

7. Artificial bee colony (ABC) algorithm

Karaboga [37] introduced the artificial bee colony (ABC) algorithm to simulate intelligent food foraging behavior of the honeybee swarm. The ABC algorithm shows excellent performance for optimizing multivariable functions as compared to other similar algorithms like genetic algorithm (GA), differential evolution (DE), and particle swarm optimization (PSO). ABC is a robust search and optimization algorithm with relatively fewer control parameters [38]. Although GA is extensively used due to its efficiency to solve the optimization problems with binary/discrete variables, it requires high computational time as well as high memory consumption to store unnecessary binary data during the conversion of a real number to binary and vice versa. The decoding method as applied in ABC algorithm requires one-line MATLAB code which directly quantizes continuous values of the variables by rounding off them. The food foraging behavior of real bees and the implementation of the algorithm have been briefly discussed in the following section.

7.1 Food foraging behavior of real bees

The constituents of the food foraging systems are the unemployed bees (UBs) and the employed bees (EBs) in a beehive and food sources (FSs) in their surroundings. Initially, all the bees are unemployed, and after they find a rich food source, they become employed. UBs are categorized into scout bees (SBs) and onlooker bees (OBs). The food foraging process is initiated when the SBs start to explore the rich food source randomly from any location by moving toward any direction of the search space. When SBs find a rich food source, it becomes an EB and returns to the hive to attract other bees by performing a special dance known as the waggle dance. Depending on the quality of the food source, the EBs recruit some bees to extract nectar from the source. The EBs abandon the current food source when the nectar of the source is finished and becomes scout bees (SBs). However, in the dancing area, OBs examine the quality and quantity of the food sources with the information provided by the EBs, and after examinations EBs select a food source. Thus during the food foraging process, exploration is carried out by SBs, and

exploitation is carried out by *EBs* and *OBs*. Due to the presence of both exploration and exploitation, ABC becomes a robust search and optimization algorithm. It is to be noted that the objective of the bees in ABC is to find out the location of the best possible food sources within the search space. Hence, the possible locations of the food sources are the possible solutions to this process. But in other swarm intelligence algorithms, e.g., particle swarm optimization (PSO), the locations of the individual agents are the possible solution within the search space. It is assumed that the number of employed bees (*NE*) and number of onlooker bees are equal in the colony and also these are equal to the number food sources (*FN*).

7.2 Implementation of ABC

In the following steps, the real bee colony behavior into the problem space is implemented:

- a. *Specifying objective*: The objective is to synthesize far-field patterns at f_0 by simultaneously minimizing SLL , SBL_{max} , and first null beamwidth ($FNBW$) or ripple (R).
- b. *Parameters to be optimized*: Depending on the requirement in an array synthesis problem, suitable independent parameters are chosen as the optimization parameter vector χ . The number of parameters in χ represents the dimension (D) of the specific optimization problem.
- c. *Defining the cost function*: According to the design parameters discussed above and multiple objectives of the synthesis problem, the cost function is defined as

$$\psi(\chi) = \sum_{h=0}^{h=2} W_h \cdot H(|\delta_{hd}| - |\delta_h|) \cdot (\delta_{hd} - \delta_h)^2 \quad (27)$$

where δ_h with $h = 0, 1, \text{ and } 2$ are the instantaneous values of different parameters of the desired patterns, while δ_{hd} is the desired values of the specific parameters. For all examples as considered in Section 8, δ_0 is the maximum SLL (SLL_{max}) of the pattern at f_0 and δ_1 is the value of SBL_{max} among the first five sidebands. But, for the first two examples, δ_2 represents $FNBW$, and, for the third case, it is the ripple level of the flattop pattern for which the positions of δ_{hd} and δ_h are interchanged in the Heaviside step function $H(\cdot)$. " W_h " is the weighting factor for the corresponding terms. The cost function ψ in Eq. (27) depends on " D ," the independent parameters of optimization parameter vector χ . A possible set of the parameter values may be considered as a point in the search space of D dimensional coordinate system. In ABC, the cost function ψ of the optimization problem has resembled with the food sources of the bees and each possible point as its location. The solutions of the optimization problem represent locations of the food sources, whereas the corresponding value of cost function ψ due to each point in its solution set is considered as the quality of the food source:

- d. *Initialization*: The possible solution, χ_i , where $i = 1, 2 \dots FN$, of an arbitrary number of food sources is generated randomly within the search space. With FN possible locations, each with D dimension is expressed in terms of a $[FN \times D]$ matrix.
- e. *Evaluating the quality of the food source*: For all the possible solutions, the values of ψ and the corresponding fitness values, μ_i , are evaluated.

- f. *Employed bees' stage*: The greedy nature of the employed bees (EB_s) is incorporated, and the new sources (s_i) surrounding its neighborhood are generated as follows:

$$s_{ij} = \chi_{ij} + \mathfrak{R}_{ij}(\chi_{ij} - \chi_{zj}) \quad (28)$$

where $j \in \{1, 2, \dots, D\}$ and $z \in \{1, 2, \dots, FN\}$ are randomly selected column and row indexes of the position matrix and r_{ij} is any randomly generated number through $[-1, 1]$. When any parameter of the new solution crosses its lower limit, it is replaced by its predetermined minimum value (χ_{\min}^j) and for the upper limit by its maximum value (χ_{\max}^j). If, for a new solution, the value of ψ is less than the corresponding old solution, the old is replaced by the new one.

- g. *Onlooker bees' stage*: The quality of the food source is represented by the fitness value, μ_i , of the cost function, and onlooker bees select the new source by means of the probability, ξ_i , in terms of the fitness value, determined by

$$\xi_i = 0.9 \left(\frac{\mu_i}{\mu_{\max}} \right) + 0.1 \quad (29)$$

where μ_{\max} is the maximum fitness value among the current possible solutions. Like employed bees (EBs), the greedy selection is also applicable to onlooker bees (OBs).

- h. *Scout bees' stage*: In this stage, the abandonment of a food source by the employed bees is simulated. If the fitness value of the cost function is not improved during a specified number of steps called "*limit = FN*D*" [25], it is ignored, and the parameter, q_i^j , for the new solution is provided randomly through the whole search space by Eq. (30):

$$q_i^j = \chi_{\min}^j + rand(0, 1) (\chi_{\max}^j - \chi_{\min}^j) \quad (30)$$

- i. *Remembering the best solution*: The overall new best solution as mentioned in the steps "e-h" replaces the previous best, and the value is then stored.
- j. *Stopping criterion*: Steps "(e)" to "(i)" are repeated until the cost function converges to the desired value or a predetermined value of maximizing the number of cycles (MNC).

8. Design examples and discussions

The VAS-based synthesis problems that have been reported in [6, 33] are considered at first, and the QAS-based time-modulation approach is applied to realize the patterns. Here, the modulation period T_m is quantized in 10 equal discrete levels, i.e., $Q = 10$. Hence, the discrete search space for the optimization problem (τ_p) becomes $\{0.1, 0.2, 0.3, 0.4, 0.5, 0.6, 0.7, 0.8, 0.9, 1\}$.

Example 1: A 30-element UE TMLAA is placed along the x-axis with one element at the origin, and a uniform inter-element spacing of 0.7λ is considered. It is desirable in practice for such an array to feed with $\{A_p\} = 1$ and $\{\phi_p\} = 0$. Here,

$\chi = \{\tau_p\}$ is taken as the optimization parameter vector. The control parameters of ABC such as $EN = 30$, $limit = 900$ ($limit = EN \cdot D$), and $MNC = 700$ are selected as per the guidelines given in [38]. W_1 , W_2 , and W_3 are selected as 2, 1, and 1, respectively. In Eq. (27), δ_{1d} , δ_{2d} , and δ_{3d} are set as -20 , -30 , and 7 dB, respectively. The ABC optimized far-field power pattern with side lobe level (SLL) of -20.15 dB, $FNBW$ of 6.86° , and sideband levels ($SBLs$) at the first two sidebands as $SBL_1 = -30.78$ dB and $SBL_2 = -31.63$ dB, respectively, is shown in **Figure 15**.

Table 2 contains the ABC optimized values of τ_p of the elements used to obtain **Figure 15**. As compared to [6], SLL_{max} and SBL_{max} are improved by a factor of 0.1 and 0.7 dB, respectively, in the proposed work. The total sideband power is calculated by using either of the expressions derived in [14] or [39] and found to be 4.83% of the total power which is quite higher than 3.89% and 3.57% as reported in

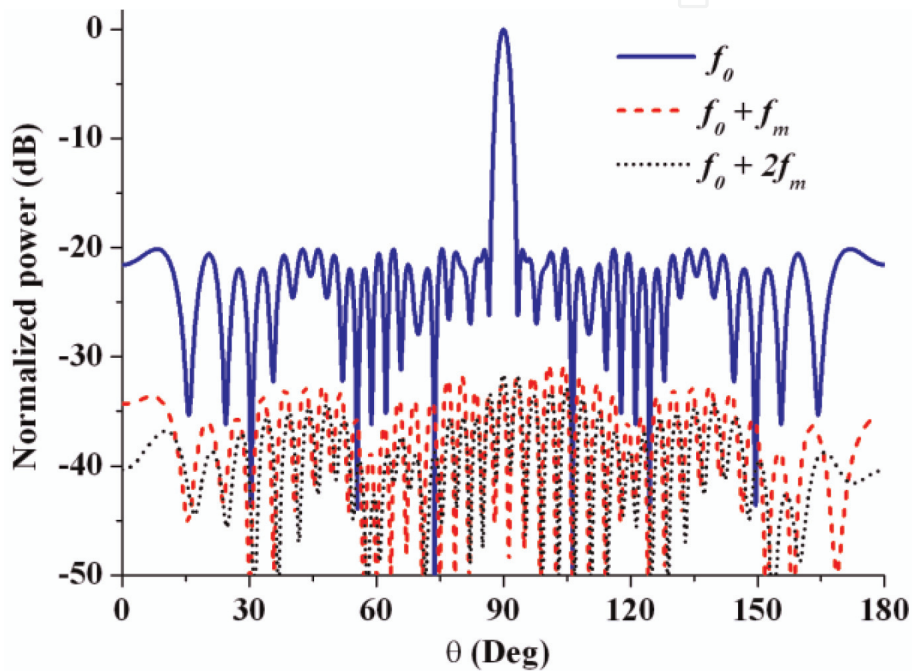


Figure 15. ABC optimized power pattern obtained by using the discrete value of τ_p of **Table 2**.

Element numbers (p)	τ_p
1	1
2	0.30
3	0.10
4–22	1
23	0.90
24	0.90
25	0.10
26	0.10
27	0.10
28	0.90
29	0.10

Table 2. Optimum discrete values of τ_p for the power pattern of **Figure 15**.

the work of [6, 40], respectively. However, the method as proposed in [40] may be utilized to reduce the waste of power in the form of sideband radiations.

Example 2: In the second example, the synthesis problem as discussed in [33] is considered. From the list of static and dynamic excitations of one-half of the linear arrays as presented in **Table 3**, Ref. [33], it was found that out of the five edge elements, only three are time-modulated to synthesize the sum pattern, whereas, for the difference pattern, time modulation is applied only on four center elements. In this work, to synthesize the sum and difference pattern, the proposed method is applied in the following way. For the UE TMLAA, the sum pattern is synthesized by taking the discrete τ_p values of five edge elements (in one-half of the array) as “ χ .” In order to compare the ABC optimized results with those of SA, during optimization, the three lower values of τ_p are rounded off to their nearest quantization levels, whereas the higher two τ_p values are kept to 1 so that the ABC optimized pattern is obtained by time modulating the same number of (i.e., three) elements as observed in SA. However, to synthesize the difference pattern, perturbation of discrete τ_p values of four center elements are considered. In Eq. (27), the same values of δ_{hd} 's as used in Example 1 are set. **Figures 16** and **17** show the ABC optimized sum and difference patterns, respectively. For optimizing the sum and difference pattern with $NE = 30$ and $limit = 450$, the ABC takes only 23 and 5 iterations, respectively (refer to **Figure 18**). The corresponding optimum discrete values of τ_p are shown in

Element numbers	1 & 30	2 & 29	3 & 28	4 & 27	5 & 26	6–11 & 25–20	12 & 19	13 & 18	14 & 17	15 & 16
τ_p Sum pattern	1	1	0.2	0.9	0.1	1	1	1	1	1
Difference pattern	1	1	1	1	1	1	0.1	0.9	0.3	0.1

Table 3.

Optimum discrete values of τ_p of ABC optimized sum and difference pattern, as shown in **Figures 12** and **13**.

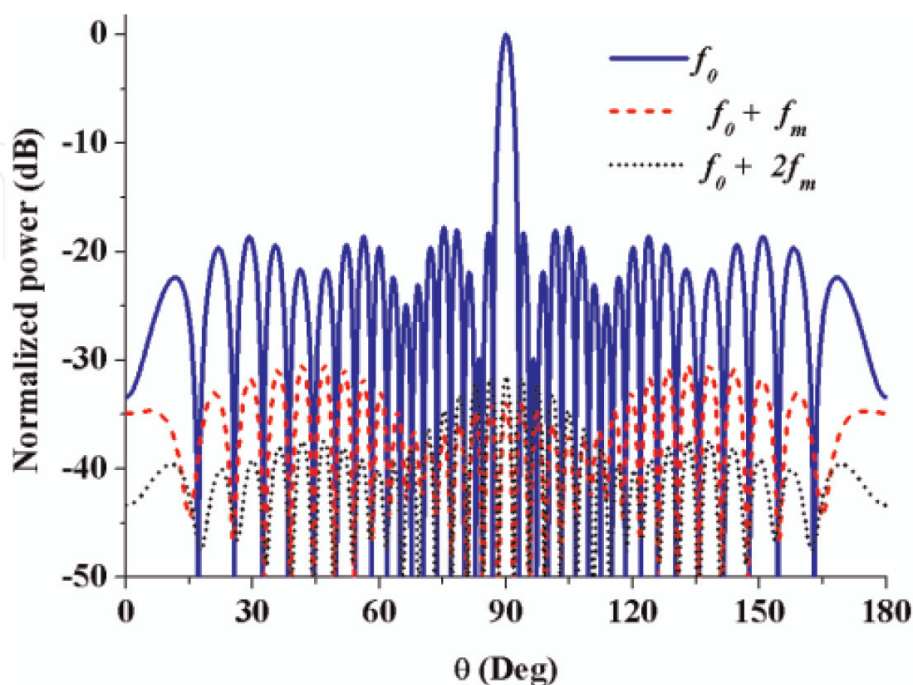


Figure 16.

ABC optimized sum pattern as obtained by time modulating the same percentage (20%) of elements as in [33]. SLL and SBL_{max} of the pattern are obtained as -17.87 and -31.44 dB, respectively.

Table 3. It can be observed that the sum and difference pattern is obtained by time modulating the same number of elements as found in [33]. As compared to [33], SLL_{max} and SBL_{max} of the sum pattern are improved by 2.03 and 1.5 dB, respectively. In case of difference pattern, the SBL_{max} is reduced by 2.37 dB with only 0.37 dB rise in SLL . Also, for both the sum and difference patterns, the amount of sideband power is found to be 3.35% and 4.69% of the total power which are 4.30% and 5.45% in the respective patterns of [33]. The $FNBW$ of ABC optimized sum

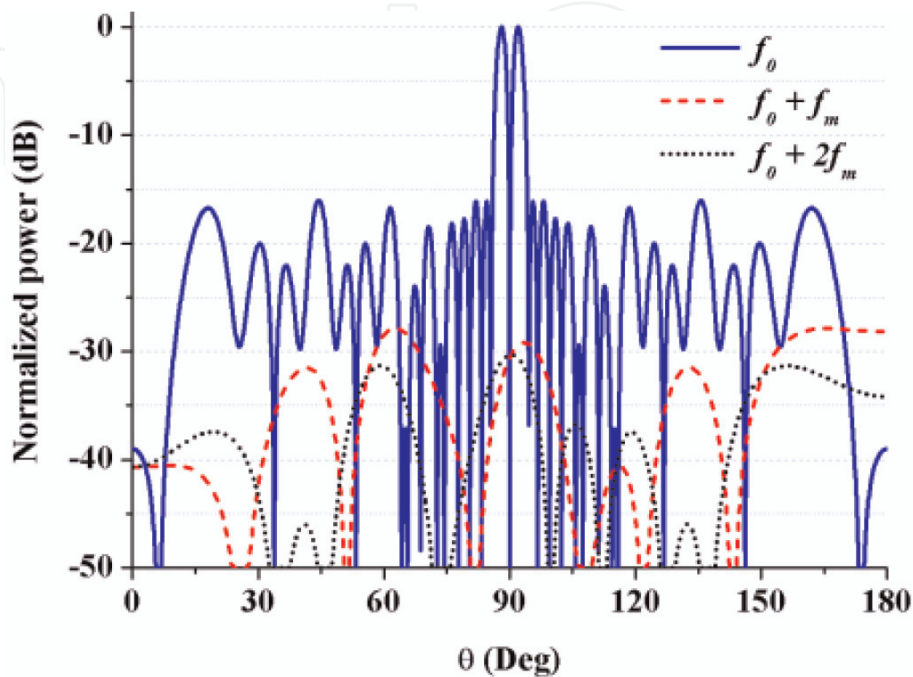


Figure 17. ABC optimized difference pattern as obtained by time modulating the same percentage (26.7%) of elements as in [33]. SLL and SBL_{max} of the pattern are obtained as -16.05 and -31.44 dB, respectively.

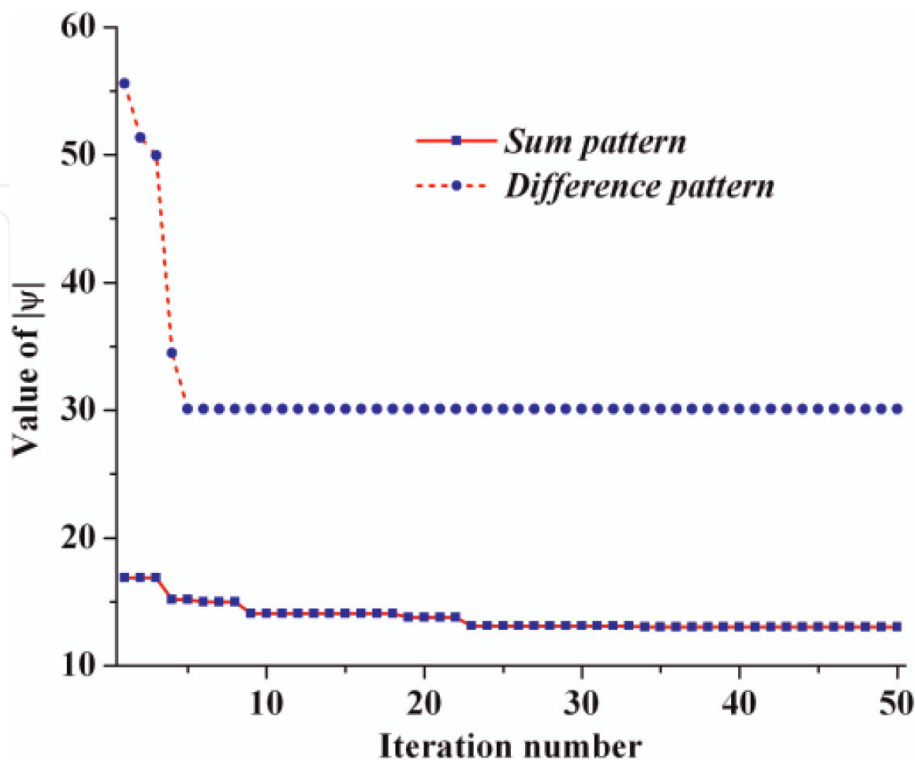


Figure 18. Convergence characteristics of ABC for the synthesized sum and difference patterns of Figures 5 and 6.

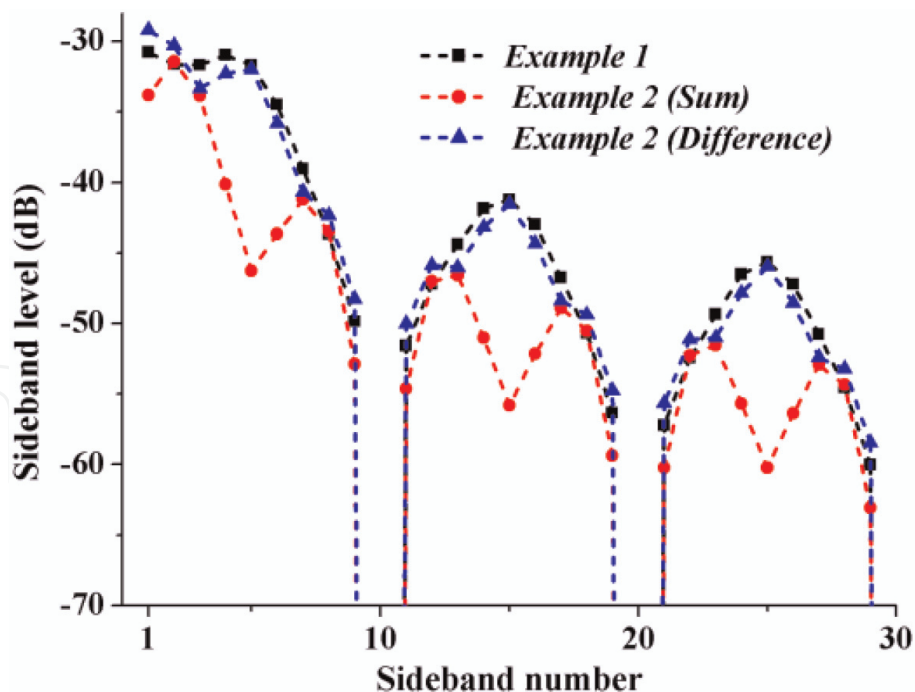


Figure 19. Sideband levels of the first 30 sidebands for the different patterns in examples 1 and 2.

pattern and difference pattern was found as 6.12 and 4.56° , respectively, which are quite comparable to 5.88 and 4.59° as for the patterns in [33].

Figure 19 shows *SBLs* of the first 30 sidebands for the synthesized patterns as considered in Example 1 and Example 2. It can be observed that at the higher sidebands also, the *SBLs* are below SBL_{max} . Further observation shows that the no radiation is produced at 10^{th} , 20^{th} , and 30^{th} sideband with quantized values of τ_p as at these harmonics the array factor expression becomes zero for all elements.

Example 3: In this example, it is shown that the same time modulator can also be used to synthesize a flattop pattern. Accordingly, a symmetrical TMLA with element number $N = 20$ and inter-element spacing $d_0 = 0.5\lambda$ is considered. Here, the objective is to synthesize a flattop pattern in the broadside direction with digitally controlled static excitation amplitudes and phases by using five digital attenuators and phase shifters. A flattop pattern with a beamwidth of 30° , maximum ripple level (R_{max}) at the flat region of less than 1 dB, and transition width of 8° is selected as the target pattern. Although such pattern with more stringent design specification is reported in [6], analog attenuators and phase shifters are required. Due to symmetry, the dimension of the parameter vector $\chi = \{A_p, \phi_p, \tau_p\}$ becomes 30. During optimization, A_p and $\phi_p \forall p \in (1, \dots, N)$ are perturbed within the search range of $(0.2-1)$ and $(-180 \text{ to } +180)$ with step sizes of $0.5/2^5$ and $360/2^5$, respectively. The number of quantization states for τ_p is selected as 20. In Eq. (27), both δ_{1d} and δ_{2d} are selected as -30 dB, while δ_{3d} is set to 1 dB. Setting $FN = 150$, the ABC parameters are obtained as in [38]. ABC converges after 2000 iterations, while the weighting factors are selected as $W_1 = 2$; $W_2 = 1$; and $W_3 = 5$. The ABC optimized 3D space pattern at fundamental frequency along with the first 30 sidebands is shown in **Figure 20**. **Table 4** contains the corresponding discrete values of A_p , ϕ_p , and τ_p . The flattop pattern in **Figure 20** is obtained with SLL , SBL_{max} , and R_{max} of -29.31 , -29.9 , and 1.22 dB, respectively. The absolute value of R_{max} is measured in the region of $75 \leq \theta \leq 105^\circ$. Hence, only 0.22 dB higher values of R_{max} are obtained by satisfying other design specification of the pattern. Also, it is observed that no such improvement in the pattern is obtained when the continuous value of τ_p is used to

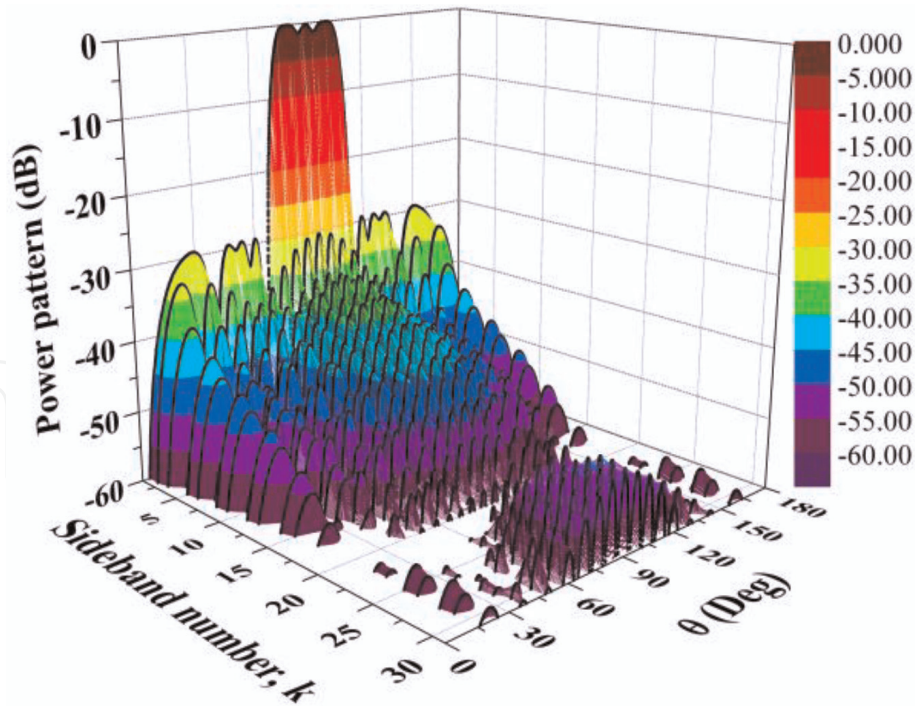


Figure 20. ABC optimized space pattern at f_0 and the first 30 sidebands. At f_0 , the flattop pattern is obtained with SLL, SBL_{max} , and R_{max} of -29.31 , -29.9 , and 1.22 dB, respectively.

Element numbers (p)	Normalized on-time, τ_p	Discrete values of excitation	
		Amplitude, A_p	Phase, ϕ_p
1 & 20	0.65	0.200	-33.75
2 & 19	0.95	0.325	-22.50
3 & 18	0.95	0.475	0
4 & 17	1	0.525	33.75
5 & 16	1	0.675	67.50
6 & 15	1	0.975	90
7 & 14	1	1	112.50
8 & 13	1	0.800	135
9 & 12	1	0.600	-180
10 & 11	1	0.700	-146.25

Table 4. Optimum discrete values of A_p , ϕ_p , and τ_p for the flattop power pattern of Figure 20.

synthesize the pattern. However, with $Q = 10$, almost the same pattern is obtained with R_{max} of 1.80 dB.

In the continuous search space of VAS time-modulation method [2, 3–6], the on-time duration of array elements can be of any value between 0 and T_m . In [2], for each time-modulated elements, the current pulse required with pulse width over the range of $(0.1T_m < t_p^{on} < 0.9T_m)$ is obtained by using the RF switches with individually controlled switching circuits. Other time-modulation schemes such as BOTS [30] and SOTS [21] need a complex programmable logic device (CPLD) for controlling the “on-off” timing of the connected switches. The continuous values of

on-time of elements can be controlled by using CPLD accurately [41, 42], but to synthesize a new antenna pattern, by realizing a new set of on-time sequence, the CPLD must be reprogrammed by completely erasing the previous set of on-time values. In contrast, the proposed VAS-QOT needs a simple circuitry as shown in **Figure 13**, where the new set of on-time sequences according to the need can be obtained simply by altering the appropriate binary input sequence to the selected inputs of the multiplexers. Thus, by fabricating the QTM in integrated circuit (IC) or by using some discrete components on a printed circuit board (PCB), TMAA switching can be done easily.

9. Conclusions

Introduction of the additional degree of freedom “time” provides flexibility in synthesizing antenna array patterns and overcomes the shortfalls of realizing the patterns through conventional array synthesis methods. Among the different time-modulation strategies, QAS can be realized through a simple digital circuit consisting of a pulse generator, simple tapped delay line with equal delay at each tap output, flip-flops, and multiplexers. This circuit can be implemented in either an integrated circuit (IC) form or in a printed circuit board and can be used as a discrete component to generate different patterns. However, as far as the nonuniform period modulation is concerned, the function of the quantized time modulator (QTM) circuit needs to be investigated, specifically to time modulate the elements with multiple frequencies which need accommodation of multiple PLLs in the circuit for the multiple frequencies. Regarding other time-modulation approaches, complexity in the switching circuit increases as per the sequence, VAS, pulse shifting, BOTS, SOTS, and NPM, respectively, while their performance in synthesizing low SLL power patterns with suppressed SBL follows the reverse order. Thus, for a time-modulation approach, the improved performance in terms of the capability of synthesizing low side lobe power patterns by suppressing harmonic signal level is obtained at the cost of complex switching mechanism. However, due to the advancement in the semiconductor technology, availability of high-speed semiconductor switches makes it possible to realize such complex switching mechanism by writing simple program code in complex programmable logic devices (CPLDs).

In all the time-modulation approaches except NPM, for the desired power pattern, optimization algorithm is required to determine the proper set of on-time sequence. The construction of suitable cost function with multiple objectives such as narrow beamwidth; low values of SLL and SBL, etc.; and the selection of corresponding weighting factors plays an important role to achieve the best possible power patterns. This chapter gives a brief fundamental insight toward all this issues.

Acknowledgements

This work is financially supported by the Ministry of Electronics and Information Technology (MeitY), Govt. of India, under Visvesvaraya Young Faculty Fellowship of Visvesvaraya Ph.D. scheme (Grant No. PhD-MLA-4(29)/2015-2016) and DST-SERB project ref. file number EEQ/2016/00836, dated January 17, 2017.

IntechOpen

IntechOpen

Author details

Sujit Kumar Mandal*, Ananya Mukherjee, Sujoy Mandal and Tanmoy Das
Microwave and Antenna Research Laboratory, Department of Electronics and
Communication Engineering, National Institute of Technology Durgapur,
Durgapur, West Bengal, India

*Address all correspondence to: skmandal2006@gmail.com

IntechOpen

© 2019 The Author(s). Licensee IntechOpen. This chapter is distributed under the terms of the Creative Commons Attribution License (<http://creativecommons.org/licenses/by/3.0>), which permits unrestricted use, distribution, and reproduction in any medium, provided the original work is properly cited. 

References

- [1] Balanis CA. Antenna Theory Analysis and Design. 3rd ed. New Delhi: A John Wiley and Sons, Inc. Publication; 2010
- [2] Kummer WH, Villeneuve AT, Fong TS, et al. Ultra-low side-lobes from time-modulated arrays. *IEEE Transactions on Antennas and Propagation*. 1963;**11**(6):633-639
- [3] Shanks HE, Bickmore RW. Four dimensional electromagnetic radiators. *Canadian Journal of Physics*. 1959;**37**(3): 263-275
- [4] Mandal SK, Mahanti GK, Ghatak R. Differential evolution algorithm for optimizing the conflicting parameters in time-modulated linear array antennas. *Progress In Electromagnetics Research, PIER B*. 2013;**51**:101-118
- [5] Yang S, Gan YB, Tan PK. A new technique for power-pattern synthesis in time-modulated linear arrays. *IEEE Antennas and Wireless Propagation Letters*. 2003;**2**:285-287
- [6] Fondevila J, Bregains JC, Ares F, et al. Optimizing uniformly excited linear arrays through time modulation. *IEEE Antennas and Wireless Propagation Letters*. 2004;**3**(1):298-301
- [7] Poli L, Rocca P, Oliveri G, et al. Harmonic beamforming in time-modulated linear arrays. *IEEE Transactions on Antennas and Propagation*. 2011;**59**(7):2538-2545
- [8] Mandal SK, Mahanti GK, Ghatak R. Synthesis of simultaneous multiple-harmonic-patterns in time-modulated linear antenna arrays. *Progress In Electromagnetics Research M*. 2014;**34**: 135-142
- [9] Li G, Yang S, Chen Y, Nie Z. A novel electronic beam steering technique in time modulated antenna arrays. *Progress in Electromagnetic Research PIER*. 2009;**97**:391-405
- [10] Song Q, Wang Y, Liu K, Zhang J, Wang Y. Beam steering for OAM beams using time-modulated circular arrays. *Electronics Letters*. 2018;**54**(17): 1017-1018
- [11] He C et al. Direction finding by time-modulated linear array. *IEEE Transactions on Antennas and Propagation*. 2018;**66**(7):3642-3652
- [12] Masoti D, Costanzo A, Del Prete M, Rizzoli V. Time-modulation of linear arrays for real-time reconfigurable wireless power transmission. *IEEE Transactions on Microwave Theory and Techniques*. 2016;**64**(2):331-342
- [13] Rocca P, Yang F, Poli L, Yang S. Time-modulated array antennas – Theory, techniques, and applications. *Journal of Electromagnetic Waves and Applications*. 2019;**33**(22):1503-1531
- [14] Bregains JC, Fondevila-Gomez J, Franceschetti G, et al. Signal radiation and power losses of time-modulated arrays. *IEEE Transactions on Antennas and Propagation*. 2008;**56**(6):1799-1804
- [15] Mandal SK, Mandal R, Mahanti GK, Ghatak R. Characteristics of sideband radiation of uniformly excited time modulated antenna arrays (TMAA) through uniform variation of ‘switch-on’ time. In: *IEEE 2011 India Conference (INDICON 2011)*. Hyderabad, India; 2011. pp. 1-3
- [16] Haupt RL. An introduction to genetic algorithms for electromagnetics. *IEEE AP Magazine*. 1995;**2**:7-15
- [17] Mandal SK, Ghatak R, Mahanti GK. Influence on side band radiation of uniformly excited TMAA during reduction of SLL of the main beam.

- In: IEEE Indian Antenna Week (IAW), Kolkata, W.B. 2011. pp. 1-4
- [18] Poli L, Rocca P, Manica L, Massa A. Pattern synthesis in time-modulated linear arrays through pulse shifting. *IET Microwaves, Antennas and Propagation*. 2010;**4**(9):1157-1164
- [19] Mandal SK, Mahanti GK, Rowdra G. Optimizing time delay of time modulated linear Array elements to reduce the side band radiation level. In: *International Conference on Signal Processing, Communications and Computing (ICSPCC)*. Hong Kong; 2012. pp. 556-559
- [20] Yang S, Gan YB, Qing A, Tan PK. Design of a uniform amplitude time modulated linear array with optimized time sequences. *IEEE Transactions on Antennas and Propagation*. 2005;**53**(7): 2337-2339
- [21] Zhu Q, Yang S, Zheng L, Nie Z. Design of a low sidelobe time modulated linear array with uniform amplitude and sub-sectional optimized time steps. *IEEE Transactions on Antennas and Propagation*. 2012;**60**(9):4436-4439
- [22] Mandal SK, Ghatak R, Mahanti GK. Design of a time-modulator to synthesize different patterns in time-modulated antenna arrays. *Journal of Electromagnetic Waves and Application*. 2014;**28**(09):1118-1130
- [23] He C, Yu H, Liang X, Geng J, Jin R. Sideband radiation level suppression in time-modulated array by nonuniform period modulation. *IEEE Antennas and Wireless Propagation Letters*. 2015;**14**: 606-609
- [24] Mandal S, Mandal SK. Harmonic power losses in time modulated arrays with non-uniform period modulation. *AEU - International Journal of Electronics and Communications*. 2019; **108**:45-52
- [25] Kanbaz I, Yesilyurt U, Aksoy E. A study on harmonic power calculation for nonuniform period linear time modulated arrays. *IEEE Antennas and Wireless Propagation Letters*. 2018; **17**(12):2369-2373
- [26] Guo J, Yang S, Chen Y, Rocca P, Hu J, Massa A. Efficient sideband suppression in 4-D antenna arrays through multiple time modulation frequencies. *IEEE Transactions on Antennas and Propagation*. 2017;**65**(12): 7063-7072
- [27] Durr M, Trastoy A, Ares F. Multiple-pattern linear antenna arrays with single prefixed amplitude distributions: Modified Woodward-Lawson synthesis. *Electronics Letters*. 2000;**36**(16):1345-1346
- [28] Chakraborty A, Das BN, Sanyal GS. Beam shaping using nonlinear phase distribution in a uniformly spaced array. *IEEE Transactions on Antennas and Propagation*. 1982;**30**: 1031-1034
- [29] Bucci OM, Mazzarella G, Panariello G. Reconfigurable arrays by phase-only control. *IEEE Transactions on Antennas and Propagation*. 1991; **39**(7):919-925
- [30] Yang S, Gan YB, Qing A, et al. Design of uniform amplitude time modulated linear array with optimized time sequences. *IEEE Transactions on Antennas and Propagation*. 2005;**53**(7): 2337-2339
- [31] Yang S, Gan YB, Qing A. Sideband suppression in time-modulated linear arrays by the differential evolution algorithm. *IEEE Antennas and Wireless Propagation Letters*. 2002;**1**:173-175
- [32] Mandal SK, Ghatak R, Mahanti GK. Design of digitally-controlled multiple pattern time-modulated antenna arrays with phase-only difference. *Annals of*

Telecommunications - annales des telecommunications. 2015;**70**(1-2):29-35

[33] Fondevila J, Brégains JC, Ares F, et al. Application of time-modulation in the synthesis of sum and difference patterns by using linear arrays. *Microwave and Optical Technology Letters*. 2006;**48**:829-832

[34] Mandal SK, Ghatak R, Mahanti GK. Minimization of side lobe level and side band radiation of a uniformly excited time modulated linear antenna array by using artificial Bee Colony algorithm. In: *Industrial Electronics and Applications (ISIEA 2011)*. Langkawi, Malaysia; 2011. pp. 247-250

[35] Pal S, Das S, Basak A. Design of time-modulated linear arrays with a multi-objective optimization approach. *Progress In Electromagnetics Research, PIER*. 2010;**23**:83-107

[36] Chen Y, Yang S, Nie Z. Improving conflicting specifications of time-modulated antenna arrays by using a multiobjective evolutionary algorithm. *International Journal of Numerical Modelling*. 2012;**25**(3):205-215

[37] Karaboga D, Basturk B. A powerful and efficient algorithm for numerical function optimization: Artificial bee colony (ABC) algorithm. *Journal of Global Optimization*. 2007;**39**(3):459-471

[38] Akay B, Karaboga D. Parameter tuning for the artificial bee Colony algorithm. In: *Proceedings of ICCCI 2009, LNCS*. Vol. 5796. Springer-Verlog. pp. 608-619

[39] Aksoy E, Afacan E. Calculation of sideband power radiation in time-modulated arrays with asymmetrically positioned pulses. *IEEE Antennas and Wireless Propagation Letters*. 2012;**11**:133-136

[40] Poli L, Rocca P, Manica L, Massa A. Handling sideband radiations in

time-modulated arrays through particle swarm optimization. *IEEE Transactions on Antennas and Propagation*. 2010; **58**(4):1408-1411

[41] Tong Y, Tennant A. Sideband level suppression in time-modulated linear arrays using modified switching sequences and fixed bandwidth elements. *Electronics Letters*. 2012; **48**(1):10-11

[42] Zhu Q, Yang S, Yao R, Nie Z. Gain improvement in time-modulated linear arrays using SPDT switches. *IEEE Antennas and Wireless Propagation Letters*. 2012;**11**:994-997